Cytoskeleton-associated protein 4 (CKAP4) affects podocyte cytoskeleton dynamics in diabetic kidney disease

Roberto Boi,[1] Emelie Lassén,[1] Alva Johansson,[1] Peidi Liu,[1] Aditi Chaudhari,[1] Ramesh Tati,[2] Janina Müller-Deile,[3] Mario Schiffer, [3,4] Kerstin Ebefors,[1] and Jenny Nyström.[1]

Conflict of interest statement

RT, EL, AC are employed by AstraZeneca. EL and AC were not employed by AstraZeneca at the time the experiments were performed. RT experiments were performed at Gothenburg University. Except for this, the authors have declared that no conflict of interest exists.

Address correspondence to: Jenny Nyström, Institute of Neuroscience and Physiology, Department of Physiology, Sahlgrenska Academy, University of Gothenburg, Box 432, 40530, Gothenburg, Sweden. jenny.nystrom@gu.se Telephone number: 031-786 33 93

RB and EL share first authorship of the manuscript.

[1] Institute of Neuroscience and Physiology, Sahlgrenska Academy, Gothenburg University, Sweden
[2] Bioscience Renal, Research and Early Development, Cardiovascular, Renal and Metabolism, BioPharmaceuticals R&D, AstraZeneca, Gothenburg, Sweden.
[3] Department of Nephrology, Friedrich-Alexander-Universität Erlangen-Nürnberg, Erlangen, Germany
[4] Mount Desert Island Biological Laboratory, Salisbury Cove, Maine, USA.

EL present affiliation: Bioscience Renal, Research and Early Development, Cardiovascular, Renal and Metabolism, BioPharmaceuticals R&D, AstraZeneca, Gothenburg, Sweden. AC present affiliation: Regulatory Affairs, AstraZeneca, Gothenburg, Sweden.

Abstract

Podocytes are kidney glomerular cells that depend on rigorously regulated cytoskeleton components and integrins to form and maintain the so-called foot processes, apparatuses that attach podocytes to the glomerular basement membrane and connect them to neighboring podocytes. In diabetic kidney disease (DKD) these foot processes are effaced as a result of cytoskeleton dysregulation, a phenomenon that gradually reduces glomerular filtration. Cytoskeleton-associated protein 4 (CKAP4) is a known linker between the endoplasmic reticulum, integrins and microtubular cytoskeleton. Since CKAP4 gene expression is downregulated in glomeruli from DKD patients but not in other chronic kidney diseases, we hypothesized a role for CKAP4 in the mechanisms leading to foot process effacement (FPE) in DKD. CKAP4 mRNA reduction in podocytes in DKD was demonstrated in human kidney biopsies. Knockdown of CKAP4 in vivo in zebrafish resulted in edema, proteinuria and foot process effacement, all typical features of DKD. Knockdown of CKAP4 in vitro led to disruption of the actin cytoskeleton and of the microtubular orientation. Moreover, it caused a downregulation of several integrins. These findings indicate that CKAP4 is crucial for foot process dynamics of podocytes. Its reduction, unique to DKD, is mechanistically connected to the pathophysiological processes leading to podocyte FPE.

Introduction

It is estimated that around 10-40% of patients with diabetes will develop diabetic kidney disease (DKD) (1). DKD is characterized by several glomerular alterations: mesangial expansion, podocyte foot process effacement (FPE), glomerular basement membrane thickening and loss of endothelial fenestrations (2). In particular, pathological alterations of the podocyte actin cytoskeleton and loss or dysfunction of several proteins in the podocyte slit diaphragm, the cell-to-cell junction structure responsible for blood filtration, have been implicated as causes of FPE (3, 4).

The cytoskeleton is composed of three distinct structures: actin microfilaments (stress fibers), intermediate filaments and microtubules. In podocytes, the actin microfilaments extend to the primary and secondary foot processes and are directly connected to the slit diaphragm, while intermediate filaments and microtubules are found mainly in the cell body and are necessary for primary foot processes formation (5-7). The three cytoskeleton components are connected at the end of adjacent major foot processes (7-9). Microtubules are hollow cylindrical structures made of α- and β-tubulin and have a polar orientation. The minus-end is found in the center of the cell and the plus-end in the periphery. Podocytes are characterized by a non-uniform microtubular polarity in that the minus-ends are also found in the cell periphery. This uniqueness is necessary for foot process formation (5). In the cell body, the microtubular network is interconnected to the endoplasmic reticulum (ER).

All three cytoskeletal components interact, hence the disruption of one affects the others. Moreover, changes that take place at the podocyte slit diaphragm can be transmitted to the nuclei via crosstalk between actin microfilaments and microtubules. This enables podocytes to respond to and send signals from and to the foot processes (10). Since microtubules are important for foot processes formation, alterations of the microtubules in the cell body might be transmitted to the peripheral actin microfilaments and cause FPE.

Given the importance of cytoskeleton architecture in podocytes, proteins that are able to interact with or modulate cytoskeletal components may have a role in the development of chronic kidney disease (CKD). One of the proteins involved in anchoring microtubules to the ER is the cytoskeleton-associated protein 4 (CKAP4) (11).

CKAP4 is a non-glycosylated, 63 kDa type-II integral protein that was first discovered in the ER (12, 13), where it stabilizes and facilitates the folding of ER sheets (14, 15). CKAP4 contains a 106 amino acid long domain with ER anchoring and microtubule binding functionality (11). Overexpression of CKAP4 has been shown to increase the number of ER sheets in epithelial cells and to induce rearrangement in both ER and the microtubular network (14, 16, 17). Moreover, CKAP4 knockdown has also been shown to cause reduction of actin polymerization and increased cell motility (18). Although CKAP4 role in disease is often associated with cancer (with conflicting reports whether it should be considered a cancer suppressor or a cancer promoter molecule), (19) CKAP4 has recently been connected to vascular calcification in chronic kidney disease. Serum levels of CKAP4 were found to be elevated in patients with CKD of different etiology when compared to healthy patients with normal renal function, and CKAP4 was found to be cause nuclear translocation of YAP (Yes associated transcriptional regulator). (20) Cytoplasmic YAP regulates cell transduction of mechanical stimuli by interacting with actin and integrins (21, 22), connecting again CKAP4 with cytoskeleton dynamics.

Since both depletion and overexpression of CKAP4 have been shown to affect the microtubular network, and as CKAP4 is also involved in actin regulation, we hypothesized that CKAP4 is essential for maintaining a functional cytoskeleton in podocytes and that loss of CKAP4 contributes to the cytoskeletal dysfunction and podocyte FPE observed in CKD.

Results

Patients with DKD have decreased glomerular CKAP4 expression.

CKAP4 expression was investigated in previously published CKD glomerular transcriptomics datasets. CKAP4 expression was significantly lower in DKD patients compared to healthy individuals. There was no significant difference in other CKD etiologies present in the datasets (Table 1) (23, 24). To validate this, CKAP4 mRNA in situ hybridization was performed on biopsies from 5 DKD patients, 4 IgAN (immunoglobulin A nephropathy) patients and 5 controls. The most pronounced expression of CKAP4 mRNA was detected in podocytes. Glomerular cells were scored for presence (purple/dark blue color) or absence (only pink/red nuclear staining) of CKAP4 mRNA (DKD: 20 glomeruli, IgAN: 22 glomeruli, control: 25 glomeruli). Sclerotic glomeruli showed absent or low CKAP4 expression and were excluded. The ratio between positive cells and total cells was used for statistical analysis. While the IgAN biopsies showed CKAP4 levels similar to the controls, glomeruli from DKD patients presented a significantly (P<0.001) lower ratio of CKAP4 positive cells (Figure 1A-D). This was in concordance with the transcriptomics data reported in Table 1. To establish a direct connection between DKD, CKAP4 and podocytes, we treated human podocytes (HPODs) with 60 mM glucose for 2 weeks. Hyperglycemia caused a reduction of CKAP4 of around 20-30% when compared to its osmotic control and untreated cells (Figure 1E).

Moreover, HPODs were treated with different concentrations of adriamycin for 24h. Adriamycin is typically used as an injury model for focal segmental glomerulosclerosis. HPOD apoptosis was confirmed by measuring cleaved versus total CASP3 (caspase 3). The level of cleaved CASP3 increased proportionally to the ADR concentration used for treatment, while total CASP3 level was stable. CKAP4 was not regulated by the treatment with adriamycin (Figure 1F).

Taken together, these results demonstrate that DKD patients have a decreased gene expression of CKAP4 and establish a direct connection between hyperglycemia and reduction of CKAP4 expression.

CKAP4 is expressed in glomerular cells in vitro and in vivo.

Expression of CKAP4 in human kidney biopsies and specifically in the glomerulus was determined by immunofluorescence (Figure 2). Co-staining of CKAP4 with Wilms' Tumor 1 (WT-1) showed expression of CKAP4 in the cell body of podocytes, while co-staining with anti-synaptopodin (podocyte foot processes marker) showed no co-localization. Partial co-localization of CKAP4 with α-smooth muscle actin (α-SMA, mesangial cell marker) and with the endothelial cell specific lectin *Ulex Europaeus* Agglutinin I was observed. There was no co-localization with the glomerular basement membrane proteoglycan agrin.

Next, the expression of CKAP4 in vitro was examined in the glomerular cell types. Western blot and qPCR analysis of CKAP4 expression in HMCs (human mesangial cells), HGECs (human glomerular endothelial cells) and HPODs showed its presence in all three cell types, with the highest expression at gene (HPODs vs HGECs, $P<0.01$, HPODs vs HMCs $P<0.01$) and protein level (HPODs vs HGECs $P<0.05$) in podocytes (Figure 3, A-B).

Immunogold labeling of CKAP4 in human kidney sections also confirmed CKAP4 presence in podocytes (Figure 3C). Immunofluorescence of cultured HPODs showed ~~immunofluorescence~~ co-localization of CKAP4 with ER marker PDIA3 (Figure 3D), in agreement with previous findings in other tissues (14, 16). The respective positions and overlaps between CKAP4 and HPOD cytoskeleton components (actin and tubulin) are shown in Figure 3E.

Knockdown of the CKAP4 homolog in zebrafish induces proteinuria.

To assess whether reduced CKAP4 expression affects the filtration barrier function, the zebrafish homolog of CKAP4 was knocked down in a zebrafish model using a morpholino (MO) blocking mRNA translation. CKAP4 MO induced proteinuria in a dose-dependent manner (30 µM: $P<0.05$, 50 and 75 µM: $P<0.001$, compared to control MO) (Figure 4A). CKAP MO zebrafish developed edema. Edematous phenotypes were assessed and quantified as described previously (from P1, no edema, to P4, severe edema) (Figure 4, B-C) (25-27).

Glomerular morphology was investigated using TEM. The CKAP4 MO group presented with podocyte FPE, whereas zebrafish injected with control MO showed normal podocyte morphology (Figure 4D). Quantification of foot processes in control MO and CKAP4 MO treated zebrafish was performed as previously described (28) and showed an increase of partially effaced (from 13 to 24%) and completely effaced (from 1 to 11%) foot processes in the CKAP4 MO group (Figure 4E). CKAP4 MO KD was confirmed with mass spectrometry (Figure 4F, Supplemental Table 1). Downregulated CKAP4 (-90%) was detected in both the CKAP4 MO versus control MO and CKAP4 MO versus untreated comparisons (in both cases $P < 0.001$).

Knockdown of CKAP4 in podocytes alters the morphology of actin filaments, microtubules and of the ER.

Since CKAP4 is known to anchor the microtubular cytoskeleton component to the ER, loss of actin cytoskeleton (stress fiber structures) is associated with podocyte FPE, and both structural components are connected at the major foot process level in podocytes, we hypothesized that a decreased expression of CKAP4 would affect both microtubules and actin cytoskeleton. To

verify this, we examined the morphology of ER, microtubules (tubulin) and actin microfilaments (stress fibers) in CKAP4 KD HPODs.

Following lentiviral KD, CKAP4 gene expression was reduced by over 90% (Supplemental Figure 1A), while the protein level was only halved, likely due to a slow protein turnover time, as observed earlier (15).

We examined the expression of ER marker PDIA3 using immunofluorescence and western blot to assess ER stress levels since the reduction of CKAP4 limits the number of anchoring points between ER and the cytoskeleton. PDIA3 distribution and hence the ER morphology was modified by CKAP4 KD with the ER structures appearing to be irregularly dispersed in CKAP4 KD cells when compared to untreated cells (Figure 3D) and scrambled virus treated (scr) cells (Figure 5A). However, PDIA3 protein level was not quantitatively affected by CKAP4 KD (Figure 5B). ATF6α (Activating Transcription Factor) was used to assess ER stress (Figure 5C) (29, 30). No changes in total (100 kDa) nor cleaved ATFα (36 kDa) were seen, concluding that CKAP4 KD does not cause ER stress.

Anti-tubulin and phalloidin stainings were used to visualize microtubules and actin microfilaments. CKAP4 KD HPODs showed loss of microtubules traversing the cell and appearance of cortical (towards the cell periphery) and concentric structures (inside of the cell). Actin fibers were also rearranged in a cortical manner and the stress fibers were reduced (Figure 6A). The protein levels of α-actinin 4 (ACTN4) and α- and β-tubulins (TUBA/B) showed no difference between the KD and scr cells (Figure 6, B and C), implying that the change was morphological but not quantitative.

Apart from cortical actin and reduced number of stress fibers, CKAP4 KD podocytes showed a 33% reduction in cell area in respect to scr cells (Figure 6D), while HPODs overexpressing CKAP4 presented an overall normal phenotype (Figure 6E). Cells positive for stress fibers were

counted as “1”, otherwise as “0”, according to the method used by Buvall et al (31). A minimum of 64 podocytes were evaluated at multiple random positions in each cell culture dish for each condition. The loss of stress fibers in CKAP4 KD cells was clear (Figure 6F) when compared to both untreated and scr control. Conversely, although CKAP4 overexpression (OE) was substantially increased (Supplemental Figure 1B), it did not cause stress fiber loss when compared to OE control (Figure 6F). Finally, CKAP4 KD did not affect HPODs viability when compared to scr and untreated cells (Figure 6G). Although a limited HPOD detachment was observed, there was no sign of apoptosis in CKAP4 KD HPODs when compared to untreated and scr controls (data not shown).

Knockdown of CKAP4 affects cytoskeleton-related pathways.

Mass spectrometry based (LC-MS/MS) proteomic analysis of CKAP4 KD and OE in HPODs was conducted to identify signaling pathways affected by altered CKAP4 expression. The principal component analysis (PCA) plots clearly show that only the CKAP4 KD cells could be separated from scr control and untreated cells (Supplemental Figure 2).

Ingenuity pathway analysis (IPA) of the comparison between CKAP4 KD and scr cells, revealed that eight of the top 20 regulated pathways were related to cytoskeleton regulation (Table 2, Supplemental Table 2).

The proteomic analysis identified an ongoing complex cytoskeletal remodeling in CKAP4 KD HPODs. The diagram in Figure 7A illustrates the dysregulation of actin (ACT), microtubules (MT) and integrin (ITG) dynamics happening in CKAP4 KD cells. The lists of proteins used for the proteomics analysis in Figure 7, A and B, are reported in Table 3.

While the actin cytoskeleton and the tubulins were not quantitatively regulated (Figure 7, A and B), the integrin pool was severely affected with 8 of the 12 identified integrins significantly downregulated (Figure 7C). Integrin related proteins were affected as well: Talin (TLN1),

RAP1A/B and its modulator RAPGEF6 (GEF, guanine nucleotide exchange factor) were all downregulated. This means that integrin activation is blocked (RAP1) and actin/integrin connection is hindered in CKAP4 KD HPODs (TLN1).

For the actin cytoskeleton, we found downregulation of ARHGEF7, ARHGAP18 (GAP, GTPase activating protein), ARHGAP29, ARHGAP1, and upregulation of ARHGEF10L. These are all modulators of the main three GTPases responsible for actin dynamics (RHOA, CDC42, RAC1) in podocytes. Perturbation of GTPases activity is known to modify the shape of the actin cytoskeleton and produce a dysfunctional phenotype (32, 33). Furthermore, CFL (Cofilin) 1 and 2 (that facilitate the movement of actin filaments by depolymerizing F-actin), and RHOC (a GTPase that regulates actin depolymerization), are downregulated as well, while profilin-1 (PFN1, involved in F-actin polymerization) was upregulated.

For what concerns the microtubules, only TUBA4A and TUBBA4 were downregulated, but generally the pool of tubulins was stable after CKAP4 KD (see TUBA/B in Figure 6C). Three members of the gamma tubulin ring complex (γ-TuRC, which prompts *de novo* synthesis of microtubules) (34) showed a trend of upregulation (+15-20% for TUBGCP3, TUBGCP5 and TUBGCP6). Interestingly, we found downregulation of microtubules-related and regulatory proteins CLASP1 (Cytoplasmic Linker Associated Protein 1), DST (dystonin), and MAP1A (Microtubule associated protein 1A) in CKAP4 KD cells.

MAP1A and DST were used for a validation of the proteomics data, as the former is known to stabilize the structure of microtubules, while the latter is a crosslinker between actin fibers and microtubules. The expression of both proteins was significantly reduced in CKAP4 KD cells, as confirmed by western blot (Figure 7D).

Thus, loss of stability and interaction with the microtubular and actin cytoskeleton, as well as loss of anchoring points (integrins) could be behind the shift in phenotype of CKAP4 KD HPODs shown in Figure 6A.

To further evaluate the connection between CKAP4 and DKD, the proteomics data was validated against glomerular transcriptomics data from DKD patients (Supplemental Table 3) (23, 24, 35). The regulation of actin and microtubule cytoskeleton, integrins and integrin modulators occurring in DKD glomeruli was in line with our findings in CKAP4 KD HPODs. We conclude that CKAP4 KD negatively impacts the cytoskeleton regulation in podocytes, affecting integrins and their signaling quantitatively and forcing the reshaping of actin fibers and microtubules filaments via a complex dysregulation of their modulators.

CKAP4 KD causes a depletion of integrins.

Since the pool of integrins was quantitatively affected in the CKAP4 KD, we decided to validate the decrease using both immunofluorescence imaging and western blot and investigated the mechanism behind their reduction. Immunofluorescence showed a decrease of total and active β1 integrins in CKAP4 KD cells, alongside the previously shown actin cytoskeleton dysregulation (Figure 8A). Western blot analysis confirmed downregulation of integrins ITGB1 (total and active; CKAP4 KD vs scr, KD vs untreated control comparisons: $P<0.001$), ITGA3 (both: $P<0.001$), ITGAV (KD vs scr: $P<0.01$, KD vs untreated: $P<0.001$), ITGB3 (both: $P<0.05$), ITGB5 (KD vs scr: $P<0.05$, KD vs untreated: $P<0.01$) and of RasGTPase RAP1A/1B (KD vs scr: $P<0.01$, KD vs untreated: $P<0.001$), an activator of integrin clustering (Figure 8, B and C). Talin 1 (TLN1), an integrin activator involved in the actin/integrin connection, was also significantly downregulated in CKAP4 KD HPODs in respect to untreated and scr cells (both, $P<0.001$).

The transcription factor forkhead box protein (FOX) M1 was downregulated at both gene ($p>0.001$) and protein level ($p>0.01$) in CKAP4 KD cells compared to untreated and scr controls (Figure 8D). FOXM1 has been reported as transcription factor for ITGB1 (36), and CKAP4 as a regulator of FOXM1 expression and activation (37-39). In conclusion, CKAP4 KD can cause

a decrease in the expression of at least ITBG1 by limiting the expression of FOXM1, thus CKAP4 KD can mechanistically affect the integrin pool.

All considered, the results strongly suggest that CKAP4 is a regulator of integrin dynamics in podocytes.

Discussion

The podocyte cytoskeleton is vital for the maintenance of podocyte structure and function. Several glomerular diseases, such as DKD, present with podocyte FPE leading to proteinuria and subsequent loss of renal function. In this study we have investigated the cytoskeleton-related function of CKAP4 in podocytes both under physiological conditions and in disease. CKAP4 mRNA was downregulated in glomeruli from DKD patients in two different datasets (23, 24). This downregulation was confirmed in renal biopsies from DKD patients and was not present in glomeruli from IgAN patients. Moreover, HPODs exposed to hyperglycemia showed a significant decrease of CKAP4 expression at protein level and a treatment with adriamycin, which is used as an injury model for FSGS, did not cause a reduction of CKAP4 in cultured HPODs.

CKAP4 was expressed by all three glomerular cell types, with podocytes displaying the highest expression. CKAP4 was present in the podocyte cell body, specifically co-localized with ER marker PDIA3. This is consistent with early findings about CKAP4 and its role as a linker between ER and microtubules (14).

To gain insight into the role of CKAP4 in glomerular function, the zebrafish CKAP4 homolog was knocked down. Zebrafish is a valuable model for chronic kidney disease because of the simplicity of its kidney anatomy, the possibility to obtain KD via morpholinos, and its translatability (40-43). CKAP4 KD in zebrafish induced podocyte FPE and proteinuria, pointing at an important role for CKAP4 in podocyte function.

Next, CKAP4 was knocked down in HPODs in vitro causing cytoskeleton rearrangement and loss of integrins. Furthermore, CKAP4 KD affected the ER shape causing the loss of regular ER patterns but did not cause an increment in ER stress. Proteomics analysis of CKAP4 KD HPODs confirmed that integrin signaling, actin and microtubule dynamics were the main regulated pathways. The proteomics analysis was extensively validated in silico against two

different glomerular DKD transcriptomic datasets, with a clear overlap of pathways regulating cytoskeleton dynamics, as well as in vitro with immunofluorescence and western blot.

In podocytes, the actin cytoskeleton connects to the microtubular network in the primary foot processes, linking them to the cell body. Microtubules are at one end linked to actin, at the other end anchored to the ER via CKAP4. Podocyte microtubules are arranged with a double orientation, allowing transport and elongation towards and away from the foot processes (5, 44). For instance, microtubular-based transport of Wilms tumor 1 interacting protein (WT1P) from foot processes to nuclei in podocytes has been shown in LPS treated mice and cultured podocytes. WT1P translocation caused actin cytoskeleton rearrangement, which was transmitted directly from the periphery to the nucleus (10). CKAP4 KD in HPODs in vitro led to substantial changes in the microtubular orientation and loss of actin stress fibers. ER morphology was also affected, with loss of regular phenotype in favor of more dispersed patterns. Loss of stress fibers is a clear sign of podocyte damage. A reduction of the cellular area was also present in the CKAP4 KD HPODs, but the viability of the cells remained unchanged. The proteomics data from the CKAP4 KD HPODs revealed that 8 out of the 20 most regulated pathways were related to cytoskeleton dynamics, further supporting the connection between cytoskeleton modifications and CKAP4. CKAP4 overexpression did not influence the phenotype of podocytes.

To explore the processes leading to the actin cytoskeleton rearrangement, alpha-actinin 4 (ACTN4) protein level was investigated. ACTN4 is responsible for bundling and crosslinking actin filaments (4, 45). Increased levels of ACTN4 have been reported in podocytes with FPE, and there is an association between aberrant ACTN4 forms, proteinuria and effacement (4). No variation in ACTN4 protein expression was found, thus the variation of morphology of the actin cytoskeleton is likely to depend on its modulators (cofilins, profilins and small GTPases regulators), as suggested by the proteomics pathway analysis. Moreover, CKAP4 KD showed

reduction of Rac-1, RhoC and many GAPs and GEFs that regulate RhoA, Rac-1, Cdc42 and Rap-1 signaling. This might underline the destabilization of focal adhesions, stress fibers, loss of lamellipodia structures and alterations of the integrin clustering.

We did not observe any variation in the protein level of (total) tubulin α-β (TUBA/B). Conversely, components of the γ-TuRC complex, responsible for microtubular *de novo* generation (34), showed a trend of upregulation in the proteomics analysis. An increase of γ-TuRC would normally presuppose a concomitant global increase of all tubulins (46). However, we did not observe any increase in our experiments. A potential explanation is that podocytes react to microtubular delocalization by prompting the generation of new microtubules, hence the increase in γ-TuRC.

Dystonin (DST), a protein that acts as spacer and crosslinker between microtubules and actin cytoskeleton (47), was reduced in CKAP4 KD podocytes. This is consistent with findings in the glomeruli of DKD patients (23, 24, 35). Microtubule-associated proteins MAP1A, MAP1B, MAPT (Tau), and MAP1S are also able to link microtubules and actin. MAPT knockout causes glomerular damage and shifts podocytes towards a motile phenotype in mice, with microtubule loss by depolymerization (48, 49). Only MAP1A was identified in our proteomic dataset. MAP1A was downregulated in CKAP4 KD cells, in concordance with what was found in the DKD validation datasets.

The integrin signaling pathway was highly regulated in CKAP4 KD cells, as the integrin pool was found to be severely depleted in CKAP4 KD podocytes. Integrins in podocytes create a dynamic link to the extracellular matrix and provide attachment to the basement membrane. For instance, α3β1 integrins bind to laminin, α1β1 and α2β1 to collagen IV (50). In the foot processes, integrins connect directly to the actin cytoskeleton and influence podocyte structure and phenotype. In a mouse model, integrin β1 podocyte-specific KD caused progressive podocyte loss and end-stage renal failure (51). Decreased expression of α3β1 integrins has been

reported in podocytes switching to a motile phenotype in vitro (52). Similar observations have been made in rat models of DKD and in diabetic patients with or without DKD (53-55). Our data reinforces these earlier findings: β1 integrin was downregulated in CKAP4 KD and podocytes shifted towards a motile phenotype, as indicated by the loss of stress fibers. CKAP4 KD interferes with integrin activation (via Talin 1 downregulation), clustering (downregulation of RAP1 and its modulators ARHGAP29 and RAPGEF6). Moreover, Talin 1 links the integrins to the actin cytoskeleton so its reduction destabilizes the connection between these two cytoskeletal components. Loss of integrins might result in podocyte FPE and detachment from the glomerular basement membrane, typical hallmarks of podocyte injury in CKD (51, 56, 57). A possible explanation for the loss of integrins in CKAP4 KD is through downregulation of transcription factor FOXM1. Expression and activation of FOXM1 appears to be regulated by CKAP4, which in turn is a transcriptional factor for ITGB1 (36-39). In CKAP4 KD cells, FOXM1 was significantly downregulated at gene and protein levels and thus it could not be activated to stimulate integrins transcription. Interestingly, FOXM1 is downregulated in glomeruli from DKD patients compared to glomeruli from normal healthy kidneys (37).

To conclude, CKAP4 anchors the microtubules to the ER stabilizing the connection between microtubules and actin. Thus, CKAP4 ensures stability of primary and secondary foot processes and consequently it appears necessary for maintaining a functional podocyte cytoskeleton. We have shown that CKAP4 KD caused dysregulation of podocyte cytoskeleton and loss of integrins in vitro, podocyte FPE and proteinuria in vivo. CKAP4 was found to be downregulated in glomeruli derived from DKD patients but not in other CKDs investigated in silico and by kidney biopsy analysis. Taking everything into account, CKAP4 has the potential to be a pharmacological target for stabilizing the cytoskeleton of podocytes specifically in DKD.

Methods

Sex as a biological variable

Sex was not considered as a biological variable in the zebrafish experiments. Though primordial germ cells exist in 24 hpf (hours post fertilization) embryos, no evidence of expression of genes driving differentiation of gonads or sex determination is present before day 8 post fertilization (58) (59). All experiments were completed at 120 hpf (5 days). Normal assessments for the adult (evaluation of the genital papilla, differences in color, shape, behavior, sex-linked SNP polymorphism analysis, gonad dissection) could not be performed in larvae (59-61). Since normal sex ratios for zebrafish have medians around 0.5 (62, 63) we assumed a similar distribution in our population.

In situ hybridization

For in situ hybridization, paraffin embedded human kidney biopsies were used. We analyzed 5 sections each from: 5 patients with DKD, 4 patients with IgAN, and 5 controls (biopsies from healthy transplantation donors). Patients' demographics for the DKD group were as follows: Age 55 (47-58) (median range); sex: 4 males, 1 female; CKD stage: I (n=1), III (n=3), V (n=1). Regarding the IgAN group we had: Age 73 (63-74); sex: 4 males, 1 female; CKD stage: II (n=5), III (n=1). Healthy controls biopsies were taken from anonymous transplantation donors. The miRCURY LNA miRNA ISH kit 8 (FFPE) was used (Qiagen) and mRNA was stained using the hsa-CKAP4 3' DIG probe. After deparaffinization, the sections were incubated with proteinase K (Sigma) for 10 min at 37 °C. After washing twice with PBS, hybridization mixture was added, and the sections were incubated for 1 h at 55 ^{0}C. The sections were washed 3 times with SSC buffer and incubated for 30 min with blocking solution. The sections were incubated with anti-DIG-AP for 1 h at room temperature, washed 3 times with PBS-T and incubated with

freshly prepared AP reaction mixture for 2 h at RT. The reaction was stopped using KTBT buffer followed by washes and then the sections were counterstained with Nuclear Fast Red solution (Merck). After dehydration, the sections were mounted using mounting medium. Images were acquired using an Axioscan 7 slide scanner (Zeiss).

Glomerular cells were scored for presence or absence of CKAP4 mRNA. In total we scored: 20 glomeruli for DKD, 22 glomeruli for IgAN, 25 glomeruli for the control group. At least 1400 cells were scored per group (60 cells per glomerulus on average). Sclerotic and pre-sclerotic glomeruli (around 35% of the glomeruli in DKD and IgAN groups) were omitted from the analysis. The ratio between positive cells and total cells was used for statistical analysis.

Immunofluorescence of kidney biopsies

Biopsies were obtained from the healthy part of kidneys of patients undergoing nephrectomy due to tumors. Frozen human kidney sections derived from those biopsies were used for immunofluorescence. A list of antibodies is given as supplemental spreadsheet. Imaging was done using an Axio Imager.Z2 LSM800 confocal microscope (Zeiss).

Western blotting

Cells lysis buffer was 50 mM Tris, 150 mM NaCl, 1% Triton X-100, pH 7.5. Lysates were mixed and centrifuged (13000 rpm, 10 min, 4 °C). The resulting supernatants were used after addition of 25% Laemmli sample buffer (Bio-Rad), 10% dithiothreitol reducing agent (Invitrogen) and heating (95 °C, 5 min). Lysates were run on stain-free TGX gels 4-15% gradient polyacrylamide gels. Proteins were transferred to PVDF membranes using the TransBlot Turbo transfer system (Bio-Rad). Membranes were blocked in TBS, 0.1% Tween 20 (TBS-T), 5% milk powder blotting grade blocker (Carl Roth) for 1 h before incubation with

primary antibody overnight at 4 °C. Membranes were washed in TBS-T (3x5 min) and incubated with secondary antibodies (1 h at room temperature). After incubation, the membranes were washed again with TBS-T (3x5 min) and developed with ECL substrate (Bio-Rad) for 5 min or fluorescent detection. The bands were visualized using the ChemiDoc Touch and ChemiDoc MP Imaging systems (Bio-Rad). A list of antibodies is given as supplemental spreadsheet.

Stain-free total-lane or housekeeping (GAPDH) normalizations were used. Unedited blots and total lane blots used for normalization calculation are provided in the supplementary file "Full unedited blots".

Cell culture

Human conditionally immortalized podocytes (HPODs, University of Bristol, UK) (64, 65) and primary human mesangial cells (HMCs, Cell Systems) were cultured as described previously (65, 66). Primary human glomerular endothelial cells (HGECs) (Cell Systems) were cultured on attachment factor (ThermoFisher) coated plates in Complete Classic Medium (Cell Systems) supplemented with 10% FBS, 1% Culture boost, 1% penicillin/streptomycin. Human embryonic kidney cells (HEK293T) were used for lentivirus production.

For the high glucose experiments, HPODs were maintained in 1 nM insulin (Tocris Bioscience) and normal 5 mM glucose after thermoshifting the cells from 33°C to 37 °C. After 2 weeks of differentiation, treatments were applied for 2 weeks, with medium changes 3 times per week. Glucose was used at a 60 mM concentration. The osmotic control was normal glucose with mannitol (Mtl) up to 60 mM. The experiment was modelled by revisiting previously published methods (66-68). The high glucose concentration and long exposure were used to achieve a model of long-term diabetes and to overcome the issue of the slow turnover of CKAP4 that was also detected with the lentiviral knockdown.

For the adriamycin (ADR, doxorubicin hydrochloride, Merck D1515) experiment, HPODs were differentiated for 2 weeks before treatment. ADR was prepared in DMSO (2 mg/ml), then diluted in RPMI 1640 medium (200 μg/ml) and administered for 24h (69-71).

TaqMan qPCR

Taqman qPCR (ThermoFisher) was used for gene expression analysis of CKAP4 in HMCs, HGECs, and HPODs, and FOXM1 expression in HPODs. RNA was purified using the RNeasy Mini kit (Qiagen) and converted to cDNA using the High-Capacity RNA-to-cDNA kit (ThermoFisher) and analyzed using the Quantstudio 7 Flex PCR system (Applied Biosystems). The endogenous control was GAPDH. All probes were from ThermoFisher.

Immunogold electron microscopy

Experiments were conducted following the method of Lindström et al (72). Biopsy tissues sections (circa 70 nm) were fixed in 0.1 M phosphate-buffered, 1% paraformaldehyde, 0.5% glutaraldehyde and processed for K11M low-temperature embedding. Anti-CKAP4 mouse primary antibody was #ENZ-ABS669-0100 (Enzo Life Sciences). Sections analysis was made using a Tecnai 10 microscope (FEI) at 100 kV acceleration voltage, images were captured using a Veleta camera (Olympus Soft Imaging Solutions). CKAP4 density in different areas of the podocytes was calculated by manual counting and the areas of podocyte bodies and foot processes were measured using ImageJ. 15 micrographs from healthy patients' glomeruli were used for the quantification.

Zebrafish animal model: proteinuria, and glomerular filtration barrier integrity tests

*Tg(-3.5fabp10a:gc-EGFP) z*ebrafish (*Danio rerio*) were mated with zebrafish that were homozygous or heterozygous for either AB (AB fish, see https://zfin.org/ZDB-GENO-960809-7#summary for description) or the nacre (nac^{w2}) background (nacre fish). Zebrafish were grown and mated at 28.5°C, eggs were collected within 30 min of spawning, with embryos maintained and handled in standard embryo raising media (27, 73).

The strain of zebrafish used simplifies the assessment of proteinuria (25). A fluorescent vitamin D-binding protein is expressed by the *Tg(-3.5fabp10a:gc-EGFP) z*ebrafish, easy to monitor in the retinal vessel plexus. This systemic fluorescence increases over time. If the glomerular filtration barrier is damaged, the fish loses plasma proteins resulting in fluorescence decrease. Proteinuria was measured by reduction of eye fluorescence using an Axiovert 200 microscope (Zeiss). Maximum fluorescence intensity was analysed in grey scale using Image J (https://imagej.nih.gov/ij/) by using the outer circle measurement of the eye (25, 27).

Transmission electron microscopy (TEM) was used to examine the morphology of the glomerular filtration barrier (120 hpf). Larvae were fixed in solution D overnight at 4 °C, washed three times in 0.1 M cacodylate buffer (pH 7.4) and post-fixed in 1% OsO4 for 1 h. Tissues were subsequently washed, dehydrated, and embedded in EPON and hardened at 60 °C for more than 16 h. Sections were then prepared for transmission electron microscopy by staining with uranyl acetate (2%) for 30 min and lead citrate for 15 min. 90 nm sections of the glomerular region were cut with a microtome and transferred to copper grids. Podocyte foot process effacement percentages were calculated according to the method described by Müller-Deile et al (28).

Zebrafish animal model: exclusion criteria and power calculations

The following exclusion criteria were used: absence of "red sac" after morpholino injection at 0 hpf (MO is injected with Phenol Red, hence a successful injection is identified by a "red sac" (74) slowly diffusing to the yolk); dead embryo at 48 hpf; no flow at 48 hpf.

The tool at https://clincalc.com/stats/samplesize.aspx was used for a priori sample size calculation. The average measurements of max eye fluorescence from the MO control group at 96 hpf was used. As it was impossible to predict the extent of the KD, a small effect size was predicted (15% reduction), with $\alpha = 0.05$ and power = 80%. The number of animals per groups needed were at least 25. The reduction detected after the experiment was performed was more than 25% (30μM ckap4 MO vs control MO).

Zebrafish animal model, morpholino ckap4 knockdown and confirmation with proteomics

ATG-blocking morpholinos (MO) were used at 30, 50, and 75 μM concentrations. The zebrafish functional homologue to human CKAP4 (75) was knocked down using the anti-*ckap4* MO (5' AGA GAG ATG GCT TGA ACT CCC 3'). A morpholino targeting a human intron mutation causing beta-thalassemia was used as negative control (5' CCT CTT ACC TCA GTT ACA ATT TAT A 3'). Both morpholinos were from Gene Tools (Philomath, OR, USA). The morpholinos were injected using a Nanoject II injection drive (Drummond Scientific, Broomall, PA) into one- to four-cell stage zebrafish embryos (27). A minimum of 32 larvae per group was injected with morpholinos.

Ckap4 knockdown was confirmed at protein level using proteomics since there are no commercially available antibodies for zebrafish *ckap4*. Three pools of untreated, 75 μM control-MO and 75 μM CKAP4-MO treated larvae (n>8) were collected at 96-120 hpf. The pooled larvae were washed in PBS and then submitted to lysis using 2.5 mm ceramic beads in

SDS gel loading buffer. 10 µg of each respective protein lysate were run on 10% NuPAGE Tris Glycine gel and digested with trypsin as previously described (76). A nano LC-MS/MS (Dionex Ultimate 3000 RLSCnano) interfaced with an Eclipse Orbitrap (both from ThermoFisher) was used for the mass spectrometry analysis using a data independent acquisition workflow (resolution was 12.000, AGC set at 3E6, ion time as auto, and MS scan range 400-1200). The ions in C-trap were sequentially isolated with 8 m/z windows, with AGC at 4E5 and ion time set to auto. The ions were fragmented using a relative collision energy of 30. MS/MS scans were recorded with a resolution of 30000. Raw data were analysed using the recommended setting in the DIA-NN 1.8.1 software (https://github.com/vdemichev/DiaNN), in library-free mode (search against a sequence database, *Danio rerio* Uniprot proteome library) and with a false discovery rate (FDR) of 1% (77). The results were analysed using Qlucore omics explorer (version 3.9, Qlucore). A protein was considered significantly regulated when FC was ± 20 %, and an FDR adjusted p value (q value) of $q<0.05$.

shRNA silencing and overexpression of CKAP4 in vitro in HPODs

Knockdown (KD) and over expression (OE) of CKAP4 was accomplished using lentiviral transfection. For KD, short hairpin RNA targeting CKAP4 mRNA (target sequence: GCAGGATTTGAAAGCCTTAAA), inserted in the pLKO.1 cloning vector, was used (Sigma-Aldrich) (78). The pLKO.1 vector with non-silencing (scrambled, scr) shRNA was used as a virus control. For OE, the CKAP4 gene was amplified with PCR using the pCMV6-AC-CKAP4-GFP vector (Origene, Rockville, MD, USA). The obtained cDNA was ligated into a VVPW-EGFP vector, placing the CKAP4 gene at the C-terminus of EGFP to generate a fusion protein with EGFP at the N-terminus (cytosolic) of CKAP4. VVPW (79, 80) is a lentiviral expression vector (Virus Vector) containing the PKG promoter region and the cis-acting posttranscriptional regulatory element of the woodchuck hepatitis virus WPRE (PKG, WPRE

promoters). The VVPW-EGFP vector was a kind gift from Dr Anna Greka at Brigham and Women's Hospital and Harvard Medical School.

The VVPW-EGFP (simply reported as VVPW in the figures) vector without insert was used as control. All vectors were amplified in *E. coli* and purified using the HiSpeed Plasmid Maxi kit (Qiagen). Lentivirus were produced in HEK293T cells by addition of envelope (CMV), packaging (VSVG) and transfer plasmid (pLKO.1 or VVPW with or without insert) to cell culture medium (DMEM 4.5 g/L glucose, Lonza, Basel, Switzerland) supplemented with 10% FBS. FuGene 6 (Promega) was used as transfection reagent. The virus-containing medium was collected 72 h post transfection and stored at -80°C.

HPODs were allowed to differentiate for 7 days at 37 °C before transduction. HPODs were exposed for 16 h to a batch dependent concentration of virus-containing medium (8-33%) using 4 μg/ml hexadimethrine bromide. HPODs were kept in culture for 7 days before the experiments.

Immunofluorescence staining and evaluation of stress fiber integrity after CKAP4 KD and OE

HPODs were fixed (4 % paraformaldehyde, 4 % sucrose in PBS, 10 min), permeabilized (0.3% triton-x in PBS, 10 minutes, 4 °C) and then blocked (PBS, 2% FBS, 2% BSA, 0.2% fish gelatin). The antibodies used were: Alexa594 anti-phalloidin (actin microfilaments/stress fibers, A12381, Invitrogen), Alexa647 anti-tubulin (microtubules, Abcam, ab195884), AMAb90988 for PDIA3 (Atlas antibodies), and HPA000792 for CKAP4 (Atlas antibodies). Secondary antibodies coupled with Alexa 488, 594, or 647 were obtained from Invitrogen. Either Prolong Diamond Antifade with or without DAPI (Life technologies) or Prolong glass Anti-fade with NucBlue (ThermoFisher) were used for mounting.

For the actin microfilament morphology, HPODs were scored according to the method used by Buvall et al (31). HPODs were counted as "1" when the actin fibers (stress fibers) were spanning the whole surface of the cell, otherwise as "0". For each condition at least 60 podocytes were evaluated at multiple random positions in each culture dish using an Axio Imager.Z2 LSM800 confocal microscope (Zeiss), at 40x or 63x magnification.

Podocyte viability after CKAP4 KD

HPODs cell viability after CKAP4 KD was investigated using Alamar blue (Invitrogen). Cells were incubated with Alamar blue solution at 37 °C and fluorescence was measured using SpectraMax i3 plate reader (Molecular devices).

Mass spectrometry of protein expression in CKAP4 KD podocytes

An Orbitrap Fusion Tribrid mass spectrometer interfaced to an Easy-nLC1000 (ThermoFisher) was used for the proteomic analysis. Proteome Discoverer version 1.4 (ThermoFisher) was used for identification of the detected proteins. Database searches were performed by Mascot search engine (Matrix Science Ltd) using the SwissProt *Homo sapiens* protein database. The results were analyzed using Qlucore omics explorer versions 3.8 and 3.9 (Qlucore).

Statistical analysis of LC-MS/MS data followed the protocol from Liu et al (81). Sample expression ratios were calculated based on average quantity of all the untreated samples. Data was evaluated using density plot and histograms to ensure the distribution properties. Group clustering was checked using principal component analysis (PCA) and hierarchical clustering. Multiple t tests were performed with Benjamin–Hochberg FDR correction (set at 5%). Since a technical variance of 10% could be observed using isobaric mass tagging reagent, ± 20% cutoff on the unlogged fold change was used. Comparisons with other omics datasets (23, 24, 35) were

performed using Qlucore omics explorer (version 3.8 and 3.9, Qlucore). Significantly regulated proteins were analysed with Ingenuity Pathway Analysis 2.3 (IPA, Qiagen).

Statistics

Normality was checked with Shapiro-Wilk test and variance equality with Levene test in GraphPad Prism (versions 8-9-10, GraphPad Software), SPSS (version 23, IBM) or Qlucore omics explorer (Qlucore). Statistical differences were investigated with 2-tailed Student's T test or Mann-Whitney tests, or using ANOVA, Kruskal-Wallis tests when comparing 3 or more groups. Error bars represent standard error of the mean (SEM), or standard deviation (SD). Refer to each respective figure legend for more details.

Study approval

This study was performed in accordance with the National Institutes of Health Guide for the care and use of laboratory animals. Use of human material was approved by the regional ethical board of Gothenburg (413-09 and 110-98). Written informed consent was collected before the collection of biopsies. Zebrafish experiments were conducted at Mount Desert Island Biological Laboratory (MDIBL) and approved by the local IACUC Committee (17-03). ARRIVE reporting guidelines were used (82).

Data availability

All data generated or analyzed is included in this article and its supplementary materials. A "Supporting data values" spreadsheet is provided, containing data values for every figure and supplemental figure. For a colour-blind friendly version of the figures in this manuscript, we suggest the use of the free cvdemulator online tool at http://hclwizard.org:3000/cvdemulator/.

HPODs CKAP4 KD proteomics data have been deposited to PRIDE repository (http://www.ebi.ac.uk/pride, with dataset identifier PXD046643), whereas the zebrafish proteomics to massIVE (https://massive.ucsd.edu/ProteoSAFe/static/massive.jsp, with dataset identifier MSV000093243). Both repositories are affiliated to the proteomeXchange consortium (https://www.proteomexchange.org).

Validation datasets used in this study are available at: http://karokidney.org/rna-seq-dn (23); https://www.ncbi.nlm.nih.gov/geo/ (GSE30122) (24) and https://www.ncbi.nlm.nih.gov/geo/ (GSE47185) (35). The latter two are also available at https://www.nephroseq.org.

Author Contribution

KE, JN conceptualized the study. RB, PL curated the proteomics dataset. Validation of proteomics data was performed by RB. EL, KE, JN acquired fundings. Formal data analysis was performed by RB, EL, PL, AC, KE. Investigation was performed by RB, EL, AJ, PL, AC, RT, JMD, KE. Project administration duties were fulfilled by KE, JN. Lab resources were offered by JMD, MS, KE, JN. Supervision was granted by JMD, MS, KE, JN. Data visualization was performed by RB, EL, PL, KE. The original draft was prepared by EL. All the authors participated in writing, reviewing and editing the manuscript. CRediT classification (https://credit.niso.org/) was used to assess the contributions.

RB and EL share first authorship based upon their equally important contributions to the project. First authorship order was based on the amount of work contributed to the study. EL

initiated the study and performed experiments; RB expanded the study, performed revision experiments and data analysis.

Acknowledgements

This study was financially supported by the Swedish Medical Research Council (9898 and 2016-01200), Njurfonden grants, John and Brit Wennerström Research Foundation, and the Sahlgrenska University Hospital Grant ALF-LUA. We acknowledge: Ida Carlsson for technical assistance, Kjell Hultenby for immunogold EM analysis, Lynne Beverly-Staggs and Patricia Schroder (at MDIBL, Maine, USA) for technical assistance with the zebrafish experiments, and Gerald DiBona for the critical review of the manuscript.

Proteomic analysis of cultured CKAP4 KD cells was performed at the Proteomics Core Facility, Sahlgrenska academy, Gothenburg University, with financial support from SciLifeLab and BioMS. Proteomic analysis of morpholino-CKAP4-KD zebrafish was performed at the Biological Mass Spectrometry Facility of the Robert Wood Johnson Medical School, Rutgers University in New Jersey, USA.

References

1. Thomas MC, Brownlee M, Susztak K, Sharma K, Jandeleit-Dahm KA, Zoungas S, et al. Diabetic kidney disease. *Nat Rev Dis Primers.* 2015;1:15018.
2. Reidy K, Kang HM, Hostetter T, and Susztak K. Molecular mechanisms of diabetic kidney disease. *J Clin Invest.* 2014;124(6):2333-40.
3. Tryggvason K, and Wartiovaara J. Molecular basis of glomerular permselectivity. *Current opinion in nephrology and hypertension.* 2001;10(4):543-9.
4. Shankland SJ. The podocyte's response to injury: role in proteinuria and glomerulosclerosis. *Kidney international.* 2006;69(12):2131-47.
5. Kobayashi N, Reiser J, Kriz W, Kuriyama R, and Mundel P. Nonuniform microtubular polarity established by CHO1/MKLP1 motor protein is necessary for process formation of podocytes. *J Cell Biol.* 1998;143(7):1961-70.
6. Pavenstädt H, Kriz W, and Kretzler M. Cell biology of the glomerular podocyte. *Physiological reviews.* 2003;83(1):253-307.
7. Vasmant D, Maurice M, and Feldmann G. Cytoskeleton ultrastructure of podocytes and glomerular endothelial cells in man and in the rat. *Anat Rec.* 1984;210(1):17-24.
8. Cortes P, Méndez M, Riser BL, Guérin CJ, Rodríguez-Barbero A, Hassett C, et al. F-actin fiber distribution in glomerular cells: structural and functional implications. *Kidney international.* 2000;58(6):2452-61.
9. Neal CR. Podocytes … What's Under Yours? (Podocytes and Foot Processes and How They Change in Nephropathy). *Frontiers in Endocrinology.* 2015;6.
10. Kim JH, Konieczkowski M, Mukherjee A, Schechtman S, Khan S, Schelling JR, et al. Podocyte injury induces nuclear translocation of WTIP via microtubule-dependent transport. *J Biol Chem.* 2010;285(13):9995-10004.
11. Zheng P, Obara CJ, Szczesna E, Nixon-Abell J, Mahalingan KK, Roll-Mecak A, et al. ER proteins decipher the tubulin code to regulate organelle distribution. *Nature.* 2022;601(7891):132-8.
12. Schweizer A, Ericsson M, Bächi T, Griffiths G, and Hauri H-P. Characterization of a novel 63 kDa membrane protein : Implications for the organization of the ER-to-Golgi pathway. *Journal of Cell Science.* 1993;104(3):671-83.
13. Schweizer A, Rohrer J, Slot JW, Geuze HJ, and Kornfeld S. Reassessment of the subcellular localization of p63. *Journal of Cell Science.* 1995;108(6):2477-85.
14. Klopfenstein DR, Kappeler F, and Hauri HP. A novel direct interaction of endoplasmic reticulum with microtubules. *EMBO J.* 1998;17(21):6168-77.
15. Klopfenstein DR, Klumperman J, Lustig A, Kammerer RA, Oorschot V, and Hauri HP. Subdomain-specific localization of CLIMP-63 (p63) in the endoplasmic reticulum is mediated by its luminal alpha-helical segment. *J Cell Biol.* 2001;153(6):1287-300.
16. Shibata Y, Shemesh T, Prinz WA, Palazzo AF, Kozlov MM, and Rapoport TA. Mechanisms determining the morphology of the peripheral ER. *Cell.* 2010;143(5):774-88.
17. Vedrenne C, Klopfenstein DR, and Hauri HP. Phosphorylation controls CLIMP-63-mediated anchoring of the endoplasmic reticulum to microtubules. *Molecular biology of the cell.* 2005;16(4):1928-37.
18. Majernick T, Chavda B, and Planey SL. Cytoskeleton-Associated Protein 4 (CKAP4) Knockdown Disrupts the Actin Filament Network in Bladder Carcinoma Cells. *The FASEB Journal.* 2017;31(S1):783.14-.14.
19. Li SX, Li J, Dong LW, and Guo ZY. Cytoskeleton-Associated Protein 4, a Promising Biomarker for Tumor Diagnosis and Therapy. *Front Mol Biosci.* 2020;7:552056.

20. Shi Y, Jin X, Yang M, Jia J, Yao H, Yuan W, et al. CKAP4 contributes to the progression of vascular calcification (VC) in chronic kidney disease (CKD) by modulating YAP phosphorylation and MMP2 expression. *Cellular Signalling.* 2022;93:110270.
21. Piccolo S, Dupont S, and Cordenonsi M. The biology of YAP/TAZ: hippo signaling and beyond. *Physiological reviews.* 2014;94(4):1287-312.
22. Rinschen MM, Grahammer F, Hoppe AK, Kohli P, Hagmann H, Kretz O, et al. YAP-mediated mechanotransduction determines the podocyte's response to damage. *Science signaling.* 2017;10(474).
23. Levin A, Reznichenko A, Witasp A, Liu P, Greasley PJ, Sorrentino A, et al. Novel insights into the disease transcriptome of human diabetic glomeruli and tubulointerstitium. *Nephrology, dialysis, transplantation : official publication of the European Dialysis and Transplant Association - European Renal Association.* 2020;35(12):2059-72.
24. Woroniecka KI, Park AS, Mohtat D, Thomas DB, Pullman JM, and Susztak K. Transcriptome analysis of human diabetic kidney disease. *Diabetes.* 2011;60(9):2354-69.
25. Hanke N, King BL, Vaske B, Haller H, and Schiffer M. A Fluorescence-Based Assay for Proteinuria Screening in Larval Zebrafish (Danio rerio). *Zebrafish.* 2015;12(5):372-6.
26. Ursu R, Sopel N, Ohs A, Tati R, Buvall L, Nyström J, et al. Glomerular Endothelial Cell-Derived miR-200c Impairs Glomerular Homeostasis by Targeting Podocyte VEGF-A. *International Journal of Molecular Sciences.* 2022;23(23):15070.
27. Hanke N, Staggs L, Schroder P, Litteral J, Fleig S, Kaufeld J, et al. "Zebrafishing" for novel genes relevant to the glomerular filtration barrier. *Biomed Res Int.* 2013;2013:658270.
28. Müller-Deile J, Dannenberg J, Schroder P, Lin M-H, Miner JH, Chen R, et al. Podocytes regulate the glomerular basement membrane protein nephronectin by means of miR-378a-3p in glomerular diseases. *Kidney international.* 2017;92(4):836-49.
29. Oslowski CM, and Urano F. Measuring ER stress and the unfolded protein response using mammalian tissue culture system. *Methods Enzymol.* 2011;490:71-92.
30. Cunard R. Endoplasmic Reticulum Stress in the Diabetic Kidney, the Good, the Bad and the Ugly. *J Clin Med.* 2015;4(4):715-40.
31. Buvall L, Rashmi P, Lopez-Rivera E, Andreeva S, Weins A, Wallentin H, et al. Proteasomal degradation of Nck1 but not Nck2 regulates RhoA activation and actin dynamics. *Nat Commun.* 2013;4:2863.
32. Matsuda J, Asano-Matsuda K, Kitzler TM, and Takano T. Rho GTPase regulatory proteins in podocytes. *Kidney international.* 2021;99(2):336-45.
33. Boi R, Bergwall L, Ebefors K, Bergö MO, Nyström J, and Buvall L. Podocyte Geranylgeranyl Transferase Type-I Is Essential for Maintenance of the Glomerular Filtration Barrier. *Journal of the American Society of Nephrology : JASN.* 2023;34(4):641-55.
34. Wu J, and Akhmanova A. Microtubule-Organizing Centers. *Annu Rev Cell Dev Biol.* 2017;33:51-75.
35. Ju W, Greene CS, Eichinger F, Nair V, Hodgin JB, Bitzer M, et al. Defining cell-type specificity at the transcriptional level in human disease. *Genome Res.* 2013;23(11):1862-73.
36. Hamurcu Z, Kahraman N, Ashour A, and Ozpolat B. FOXM1 transcriptionally regulates expression of integrin β1 in triple-negative breast cancer. *Breast Cancer Res Treat.* 2017;163(3):485-93.

37. Xu X, Zhang L, Hua F, Zhang C, Zhang C, Mi X, et al. FOXM1-activated SIRT4 inhibits NF-κB signaling and NLRP3 inflammasome to alleviate kidney injury and podocyte pyroptosis in diabetic nephropathy. *Exp Cell Res.* 2021;408(2):112863.
38. Kimura H, Sada R, Takada N, Harada A, Doki Y, Eguchi H, et al. The Dickkopf1 and FOXM1 positive feedback loop promotes tumor growth in pancreatic and esophageal cancers. *Oncogene.* 2021;40(26):4486-502.
39. Xu K, Zhang K, Ma J, Yang Q, Yang G, Zong T, et al. CKAP4-mediated activation of FOXM1 via phosphorylation pathways regulates malignant behavior of glioblastoma cells. *Transl Oncol.* 2023;29:101628.
40. Poureetezadi SJ, and Wingert RA. Little fish, big catch: zebrafish as a model for kidney disease. *Kidney international.* 2016;89(6):1204-10.
41. Outtandy P, Russell C, Kleta R, and Bockenhauer D. Zebrafish as a model for kidney function and disease. *Pediatr Nephrol.* 2019;34(5):751-62.
42. Swanhart LM, Cosentino CC, Diep CQ, Davidson AJ, de Caestecker M, and Hukriede NA. Zebrafish kidney development: basic science to translational research. *Birth Defects Res C Embryo Today.* 2011;93(2):141-56.
43. Lim S, Kang H, Kwon B, Lee JP, Lee J, and Choi K. Zebrafish (Danio rerio) as a model organism for screening nephrotoxic chemicals and related mechanisms. *Ecotoxicology and Environmental Safety.* 2022;242:113842.
44. Kobayashi N, and Mundel P. A role of microtubules during the formation of cell processes in neuronal and non-neuronal cells. *Cell Tissue Res.* 1998;291(2):163-74.
45. Michaud JL, Chaisson KM, Parks RJ, and Kennedy CR. FSGS-associated alpha-actinin-4 (K256E) impairs cytoskeletal dynamics in podocytes. *Kidney international.* 2006;70(6):1054-61.
46. Thawani A, Rale MJ, Coudray N, Bhabha G, Stone HA, Shaevitz JW, et al. The transition state and regulation of γ-TuRC-mediated microtubule nucleation revealed by single molecule microscopy. *Elife.* 2020;9.
47. Roper K, Gregory SL, and Brown NH. The 'spectraplakins': cytoskeletal giants with characteristics of both spectrin and plakin families. *J Cell Sci.* 2002;115(Pt 22):4215-25.
48. Xu W, Ge Y, Liu Z, and Gong R. Glycogen synthase kinase 3beta orchestrates microtubule remodeling in compensatory glomerular adaptation to podocyte depletion. *J Biol Chem.* 2015;290(3):1348-63.
49. Valles-Saiz L, Peinado-Cahuchola R, Avila J, and Hernandez F. Microtubule-associated protein tau in murine kidney: role in podocyte architecture. *Cell Mol Life Sci.* 2022;79(2):97.
50. Mathew S, Chen X, Pozzi A, and Zent R. Integrins in renal development. *Pediatr Nephrol.* 2012;27(6):891-900.
51. Pozzi A, Jarad G, Moeckel GW, Coffa S, Zhang X, Gewin L, et al. Beta1 integrin expression by podocytes is required to maintain glomerular structural integrity. *Dev Biol.* 2008;316(2):288-301.
52. Schordan S, Schordan E, Endlich K, and Endlich N. AlphaV-integrins mediate the mechanoprotective action of osteopontin in podocytes. *American journal of physiology Renal physiology.* 2011;300(1):F119-32.
53. Chen HC, Chen CA, Guh JY, Chang JM, Shin SJ, and Lai YH. Altering expression of alpha3beta1 integrin on podocytes of human and rats with diabetes. *Life Sci.* 2000;67(19):2345-53.
54. Kemeny E, Mihatsch MJ, Durmuller U, and Gudat F. Podocytes loose their adhesive phenotype in focal segmental glomerulosclerosis. *Clin Nephrol.* 1995;43(2):71-83.

55. Regoli M, and Bendayan M. Alterations in the expression of the alpha 3 beta 1 integrin in certain membrane domains of the glomerular epithelial cells (podocytes) in diabetes mellitus. *Diabetologia.* 1997;40(1):15-22.
56. Kretzler M. Regulation of adhesive interaction between podocytes and glomerular basement membrane. *Microsc Res Tech.* 2002;57(4):247-53.
57. Frommherz LH, Sayar SB, Wang Y, Trefzer LK, He Y, Leppert J, et al. Integrin α3 negative podocytes: A gene expression study. *Matrix Biology Plus.* 2022;16:100119.
58. Kossack ME, and Draper BW. Genetic regulation of sex determination and maintenance in zebrafish (Danio rerio). *Curr Top Dev Biol.* 2019;134:119-49.
59. Parichy DM, Elizondo MR, Mills MG, Gordon TN, and Engeszer RE. Normal table of postembryonic zebrafish development: staging by externally visible anatomy of the living fish. *Dev Dyn.* 2009;238(12):2975-3015.
60. Wilson CA, High SK, McCluskey BM, Amores A, Yan Y-l, Titus TA, et al. Wild Sex in Zebrafish: Loss of the Natural Sex Determinant in Domesticated Strains. *Genetics.* 2014;198(3):1291-308.
61. Abozaid H, Wessels S, and Hörstgen-Schwark G. Effect of rearing temperatures during embryonic development on the phenotypic sex in zebrafish (Danio rerio). *Sex Dev.* 2011;5(5):259-65.
62. Hosseini S, Simianer H, Tetens J, Brenig B, Herzog S, and Sharifi AR. Efficient phenotypic sex classification of zebrafish using machine learning methods. *Ecol Evol.* 2019;9(23):13332-43.
63. Liew WC, Bartfai R, Lim Z, Sreenivasan R, Siegfried KR, and Orban L. Polygenic sex determination system in zebrafish. *PloS one.* 2012;7(4):e34397.
64. Ni L, Saleem M, and Mathieson PW. Podocyte culture: tricks of the trade. *Nephrology (Carlton).* 2012;17(6):525-31.
65. Saleem MA, O'Hare MJ, Reiser J, Coward RJ, Inward CD, Farren T, et al. A conditionally immortalized human podocyte cell line demonstrating nephrin and podocin expression. *Journal of the American Society of Nephrology : JASN.* 2002;13(3):630-8.
66. Boi R, Ebefors K, Henricsson M, Borén J, and Nyström J. Modified lipid metabolism and cytosolic phospholipase A2 activation in mesangial cells under pro-inflammatory conditions. *Sci Rep.* 2022;12(1):7322.
67. Lay AC, Hurcombe JA, Betin VMS, Barrington F, Rollason R, Ni L, et al. Prolonged exposure of mouse and human podocytes to insulin induces insulin resistance through lysosomal and proteasomal degradation of the insulin receptor. *Diabetologia.* 2017;60(11):2299-311.
68. Stieger N, Worthmann K, Teng B, Engeli S, Das AM, Haller H, et al. Impact of high glucose and transforming growth factor–β on bioenergetic profiles in podocytes. *Metabolism.* 2012;61(8):1073-86.
69. Lu Z, Liu H, Song N, Liang Y, Zhu J, Chen J, et al. METTL14 aggravates podocyte injury and glomerulopathy progression through N(6)-methyladenosine-dependent downregulating of Sirt1. *Cell Death Dis.* 2021;12(10):881.
70. Xu C, Liu X, Zhai X, Wang G, Qin W, Cheng Z, et al. CDDO-Me ameliorates podocyte injury through anti-oxidative stress and regulation of actin cytoskeleton in adriamycin nephropathy. *Biomedicine & Pharmacotherapy.* 2023;167:115617.
71. Zhu Z, Cao Y, Jian Y, Hu H, Yang Q, Hao Y, et al. CerS6 links ceramide metabolism to innate immune responses in diabetic kidney disease. *Nat Commun.* 2025;16(1):1528.

72. Sun J, Hultenby K, Axelsson J, Nordström J, He B, Wernerson A, et al. Proximal Tubular Expression Patterns of Megalin and Cubilin in Proteinuric Nephropathies. *Kidney Int Rep.* 2017;2(4):721-32.
73. Hentschel DM, Mengel M, Boehme L, Liebsch F, Albertin C, Bonventre JV, et al. Rapid screening of glomerular slit diaphragm integrity in larval zebrafish. *American journal of physiology Renal physiology.* 2007;293(5):F1746-50.
74. Zakaria ZZ, Eisa-Beygi S, Benslimane FM, Ramchandran R, and Yalcin HC. Design and Microinjection of Morpholino Antisense Oligonucleotides and mRNA into Zebrafish Embryos to Elucidate Specific Gene Function in Heart Development. *J Vis Exp.* 2022(186).
75. Takamiya M, Weger BD, Schindler S, Beil T, Yang L, Armant O, et al. Molecular description of eye defects in the zebrafish Pax6b mutant, sunrise, reveals a Pax6b-dependent genetic network in the developing anterior chamber. *PloS one.* 2015;10(2):e0117645.
76. Wei Y, Luo H, Yee PP, Zhang L, Liu Z, Zheng H, et al. Paraspeckle Protein NONO Promotes TAZ Phase Separation in the Nucleus to Drive the Oncogenic Transcriptional Program. *Adv Sci (Weinh).* 2021;8(24):e2102653.
77. Demichev V, Messner CB, Vernardis SI, Lilley KS, and Ralser M. DIA-NN: neural networks and interference correction enable deep proteome coverage in high throughput. *Nat Methods.* 2020;17(1):41-4.
78. Moffat J, Grueneberg DA, Yang X, Kim SY, Kloepfer AM, Hinkle G, et al. A lentiviral RNAi library for human and mouse genes applied to an arrayed viral high-content screen. *Cell.* 2006;124(6):1283-98.
79. Fedorova EVB, Lorenzo; Hanss, Basil; Gusella, G Luca. 733. Enhancement of Lentiviral-Mediated Gene Transfer in Kidney by Polycations and Detergents. *Molecular Therapy.* 2004;9:S279.
80. Fedorova E, Battini L, Prakash-Cheng A, Marras D, and Gusella GL. Lentiviral gene delivery to CNS by spinal intrathecal administration to neonatal mice. *The Journal of Gene Medicine.* 2006;8(4):414-24.
81. Liu P, Lassen E, Nair V, Berthier CC, Suguro M, Sihlbom C, et al. Transcriptomic and Proteomic Profiling Provides Insight into Mesangial Cell Function in IgA Nephropathy. *Journal of the American Society of Nephrology : JASN.* 2017;28(10):2961-72.
82. Percie du Sert N, Hurst V, Ahluwalia A, Alam S, Avey MT, Baker M, et al. The ARRIVE guidelines 2.0: Updated guidelines for reporting animal research. *Br J Pharmacol.* 2020;177(16):3617-24.
83. Hodgin JB, Borczuk AC, Nasr SH, Markowitz GS, Nair V, Martini S, et al. A molecular profile of focal segmental glomerulosclerosis from formalin-fixed, paraffin-embedded tissue. *The American journal of pathology.* 2010;177(4):1674-86.
84. Berthier CC, Bethunaickan R, Gonzalez-Rivera T, Nair V, Ramanujam M, Zhang W, et al. Cross-species transcriptional network analysis defines shared inflammatory responses in murine and human lupus nephritis. *J Immunol.* 2012;189(2):988-1001.
85. Reich HN, Tritchler D, Cattran DC, Herzenberg AM, Eichinger F, Boucherot A, et al. A molecular signature of proteinuria in glomerulonephritis. *PloS one.* 2010;5(10):e13451.

Figures and Figure legends

Figure 1

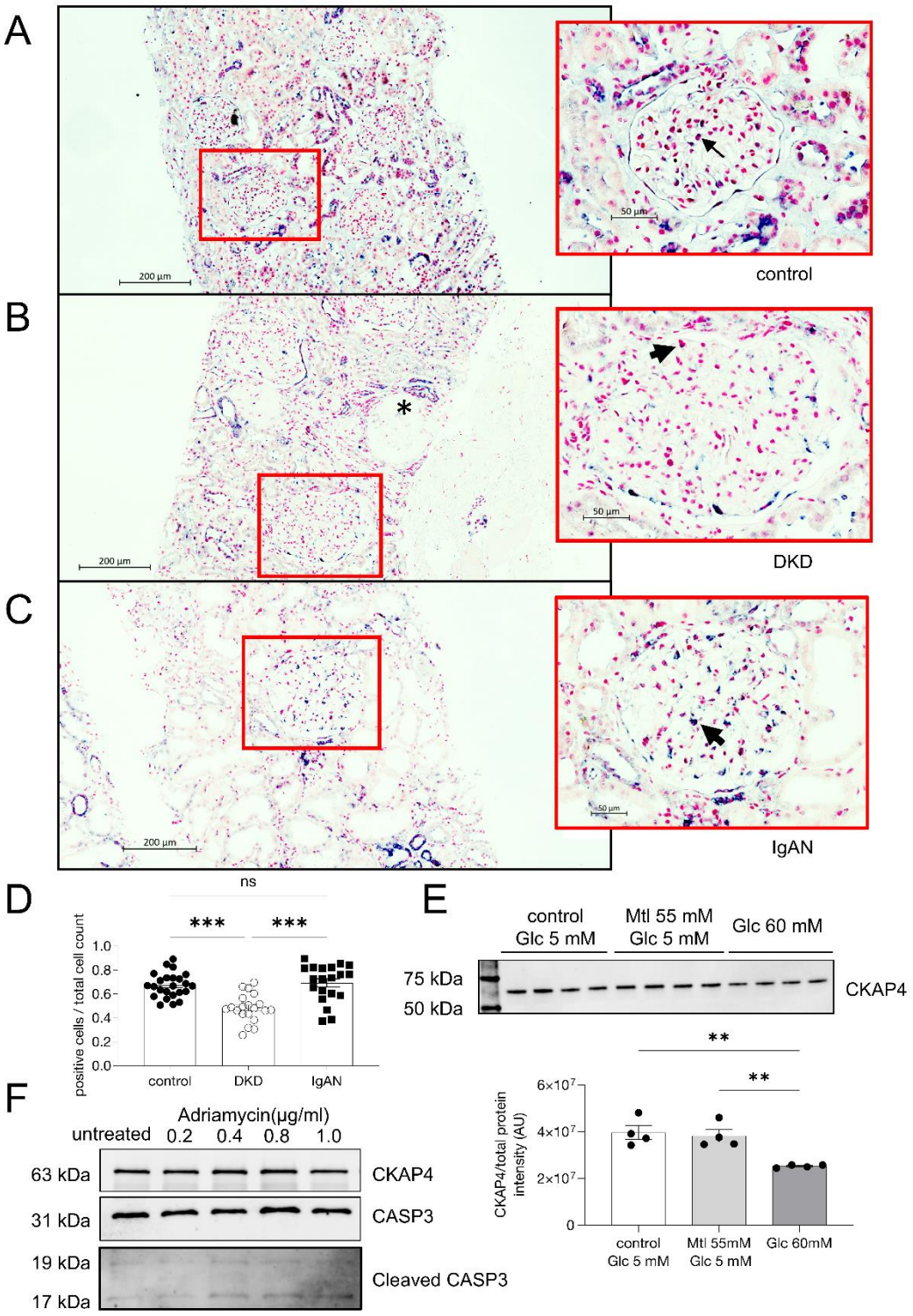

Figure 1. CKAP4 is downregulated in glomeruli in patients with diabetic kidney disease.

CKAP4 mRNA was detected using in situ hybridization in control (**A**), DKD patient biopsies (**B**) and IgAN patient biopsies (**C**). A purple/dark blue staining in the nuclear region characterizes cells positive for CKAP4 expression. Negative cells are characterized by a pink/red nuclear staining. The ratio of positive cells to total glomerular cells was used to quantify the extent of CKAP4 gene expression reduction in DKD (**D**). Completely differentiated human podocytes treated for 2 weeks with 60 mM glucose showed a 20-30% reduction of CKAP4 (**E**). Treatment of HPODs with adriamycin for 24h does not cause a decrease in CKAP4 at protein level, although cleaved CASP3 level is increased in treated cells, indicating apoptosis (**F**). Unedited/uncropped total protein blots used for normalization calculation are provided as supplementary materials.

Error bars represent average ± SEM. ** $P<0.01$, *** $P<0.001$. Panel **D**: One-way ANOVA with Tukey's multiple comparisons test, n=25 (controls), 20 (DKD), 22 (IgAN) glomeruli. 5 biopsies from 5 different patients per group (4 for IgAN) and 5 (for controls, IgAN) or 4 (for DKD) glomeruli per biopsy were scored.

Panel **E**: n=4 replicates, One-way Anova with multiple comparisons.

The asterisk in panel **B** indicates a sclerotic glomerulus. The arrows in the respective zoomed in sections of panels **A**, **B**, **C** indicate cells showing positive staining for CKAP4.

CASP3, caspase 3; CKAP4, cytoskeleton associated protein 4; DKD, diabetic kidney disease; Glc, glucose; IgAN, immunoglobulin A nephropathy, Mtl, mannitol.

Figure 2

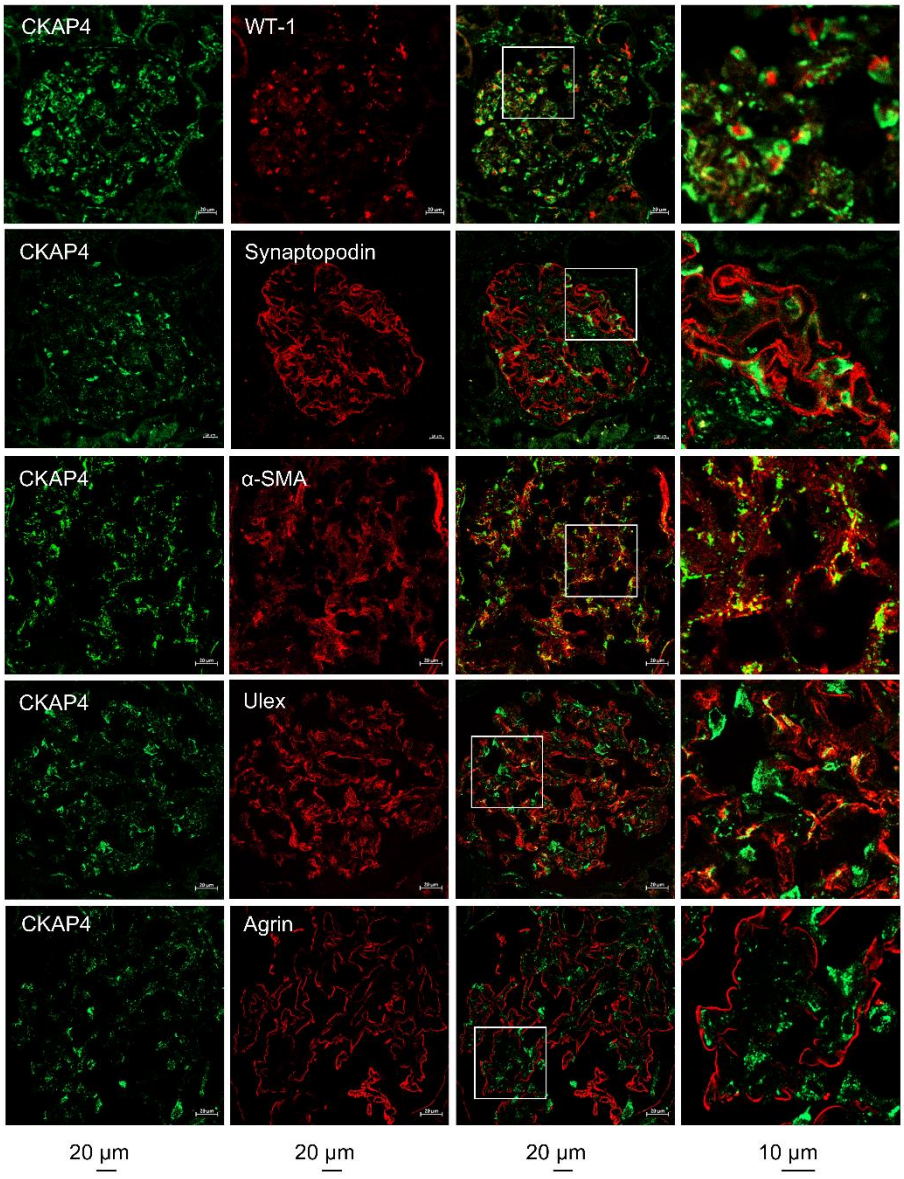
CKAP4
WT-1
CKAP4
Synaptopodin
CKAP4
α-SMA
CKAP4
Ulex
CKAP4
Agrin
20 µm
20 µm
20 µm
10 µm

Figure 2. CKAP4 is expressed in all glomerular cell types in human glomeruli.

Immunofluorescence staining of human kidney tissue for CKAP4 (green) and various markers for glomerular cells (red) to illustrate CKAP4 localization in the glomerulus.

The first column shows CKAP4 staining. The second column shows, respectively: WT-1, marker for podocyte nuclei; synaptopodin, marker for podocyte foot processes; α-SMA, marker for mesangial cells; *Ulex Europaeus* Agglutinin I, marker for endothelial cell; agrin, marker for basement membrane. The third column shows co-localization, the fourth column contains zoomed area (white squares in the third column). Representative scalebars are placed below each column. All zoomed in areas in the last column had a surface of 65 μm^2.

CKAP4, cytoskeleton associated protein 4; WT-1, Wilms tumor 1; α-SMA, smooth muscle actin.

Figure 3

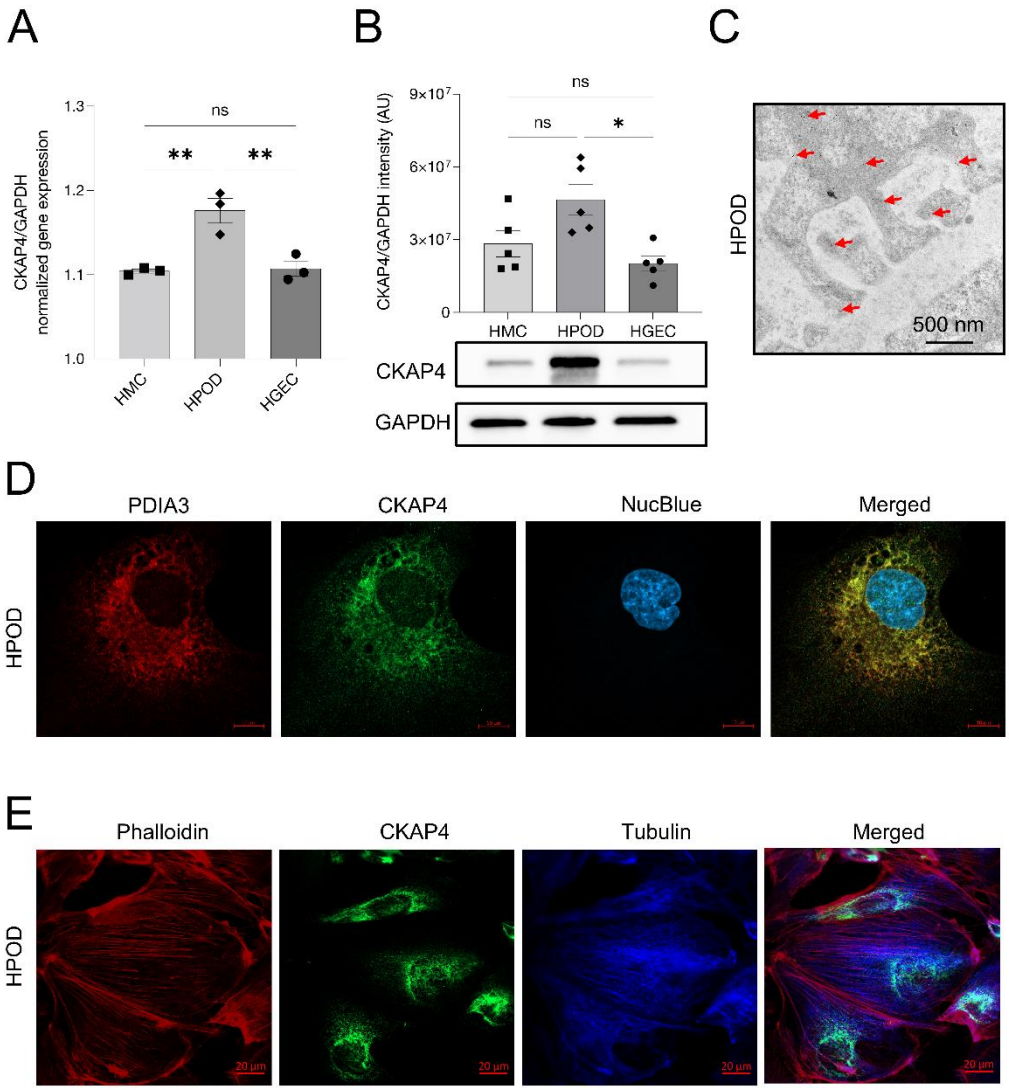
A
B
C
CKAP4/GAPDH normalized gene expression
1.3
1.2
1.1
1.0
ns
**
**
HMC
HPOD
HGEC
CKAP4/GAPDH intensity (AU)
9×10^7
6×10^7
3×10^7
0
ns
ns
*
HMC
HPOD
HGEC
CKAP4
GAPDH
HPOD
500 nm
D
PDIA3
CKAP4
NucBlue
Merged
HPOD
E
Phalloidin
CKAP4
Tubulin
Merged
HPOD
20 µm

Figure 3. CKAP4 expression and localization in glomerular cells in vitro.

CKAP4 gene expression was quantified with qPCR (**A**) and protein expression by western blot (**B**) in cultured HGECs, HMCs and HPODs, normalized against the respective GAPDH gene/protein levels. Immunogold electron micrograph of podocyte feet and major processes, red arrows point at gold particles (**C**). Immunofluorescence of PDIA3 (ER marker, red), CKAP4 (green) and DAPI (blue) show expression of CKAP4 in the ER of HPODs (**D**). Immunofluorescence of phalloidin (actin cytoskeleton, red), CKAP4 (green) and tubulin (blue) show the localization of CKAP4 in relation to cytoskeleton components (**E**).

Panel **A**: One-way Anova with multiple comparisons, n=3 per cell type. Panel **B**: Kruskal-Wallis plus Dunn post hoc test, n=5 per cell type. One representative blot is shown.

Error bars in both panels represent average ± SEM. * $P<0.05$, ** $P<0.01$.

AU, arbitrary units; CKAP4, cytoskeleton associated protein 4; HMCs, human mesangial cells; HPODs, human podocytes; HGECs, human glomerular endothelial cells; PDIA3, protein disulfide-isomerase A3.

Figure 4

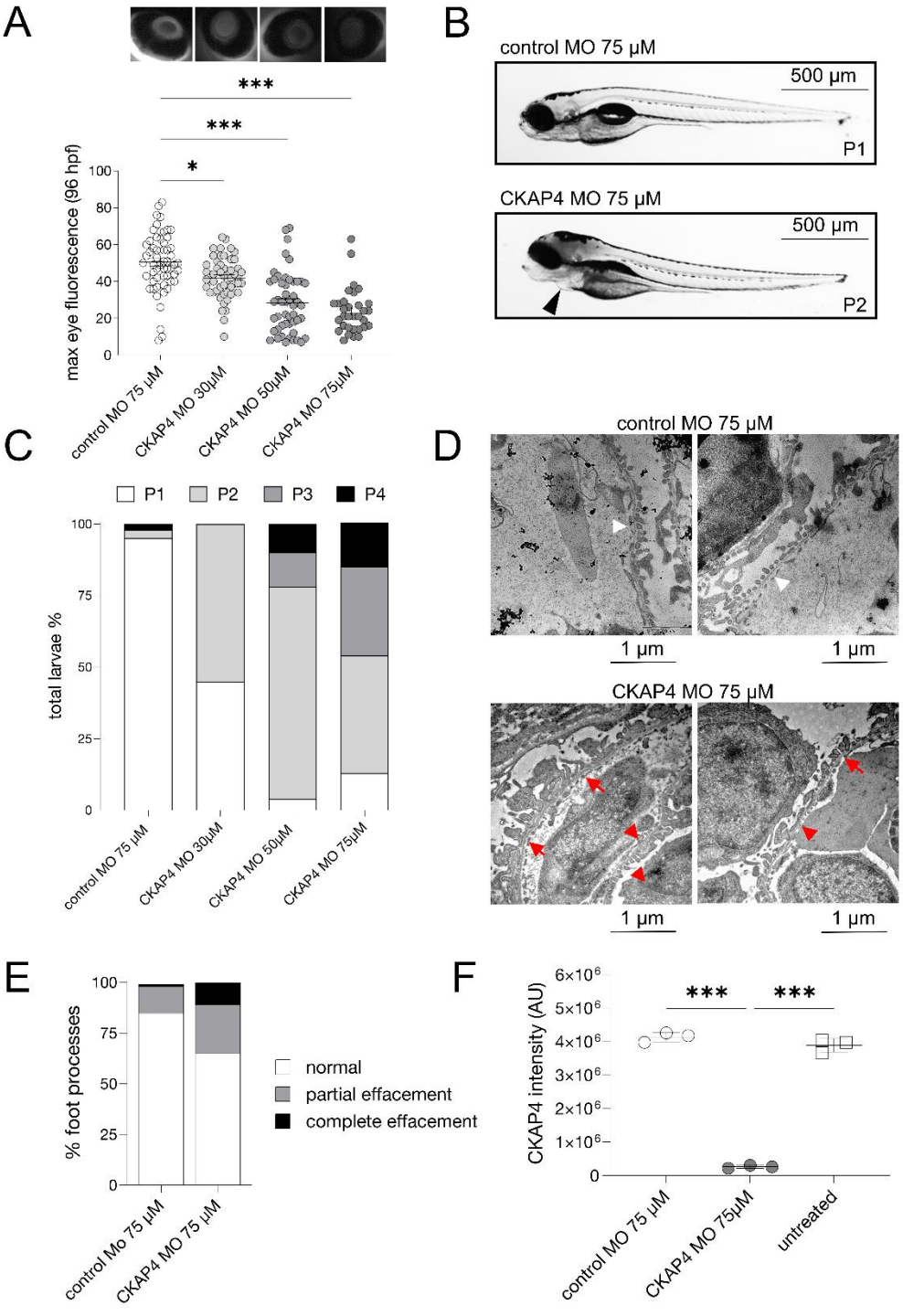
A
***
***
*
max eye fluorescence (96 hpf)
100
80
60
40
20
0
control MO 75 µM
CKAP4 MO 30µM
CKAP4 MO 50µM
CKAP4 MO 75µM
B
control MO 75 µM
500 µm
P1
CKAP4 MO 75 µM
500 µm
P2
C
P1
P2
P3
P4
total larvae %
100
75
50
25
0
control MO 75 µM
CKAP4 MO 30µM
CKAP4 MO 50µM
CKAP4 MO 75µM
D
control MO 75 µM
1 µm
1 µm
CKAP4 MO 75 µM
1 µm
1 µm
E
% foot processes
100
75
50
25
0
normal
partial effacement
complete effacement
control Mo 75 µM
CKAP4 MO 75 µM
F
CKAP4 intensity (AU)
6×10^6
5×10^6
4×10^6
3×10^6
2×10^6
1×10^6
0
***
***
control MO 75 µM
CKAP4 MO 75µM
untreated

Figure 4. CKAP4 zebrafish homologue knockdown cause proteinuria and podocyte foot process effacement.

CKAP4 was knocked down in zebrafish using MO in different concentrations, 30, 50 and 75µM MO. Proteinuria was measured by reduction of eye fluorescence (**A**). Example of normal phenotype (P1, no edema) and fish with mild edema (P2) in CKAP4 MO, the arrow points at pericardial edema (**B**). Assessment of fish phenotypes in the different groups, from P1 to P4 (severe edema) was conducted with reference to Hanke et al (25, 27) and Ursu et al (26) (**C**). Representative electron microscopy pictures of the filtration barrier of zebrafish glomeruli from control MO and CKAP4 MO (75µM). Control MO shows normal podocyte foot processes (this pattern is indicated with short white arrows) while the CKAP4 MO shows podocyte foot process effacement (partial effacement patterns are indicated with red arrows, complete effacement with short red arrows) (**D**). Quantification of podocytes foot processes effacement percentages in control MO and CKAP4 MO shows increased effacement in CKAP4 MO treated zebrafish (**E**). Validation of CKAP4 MO knockdown of CKAP4 as obtained via proteomics (**F**).

Panel **A**: a minimum of 32 larvae per group was used. Error bars: average ± SEM. * $P<0.05$, *** $P<0.001$, Mann-Whitney test. Panel **E**: n=336 (control MO), n=319 (CKAP4 MO) foot processes were counted, from n=14 (control MO) and n=8 (CKAP4 MO) independent images per group. Panel **F**: three independent experiments were performed, each treatment in each replicate is derived from lysate of a minimum of 8 pooled embryos. Error bars in both panels represent average ± SEM. *** $P<0.001$, one-way ANOVA with Tukey's multiple comparison test. CKAP4, cytoskeleton associated protein 4; MO, morpholino.

Figure 5

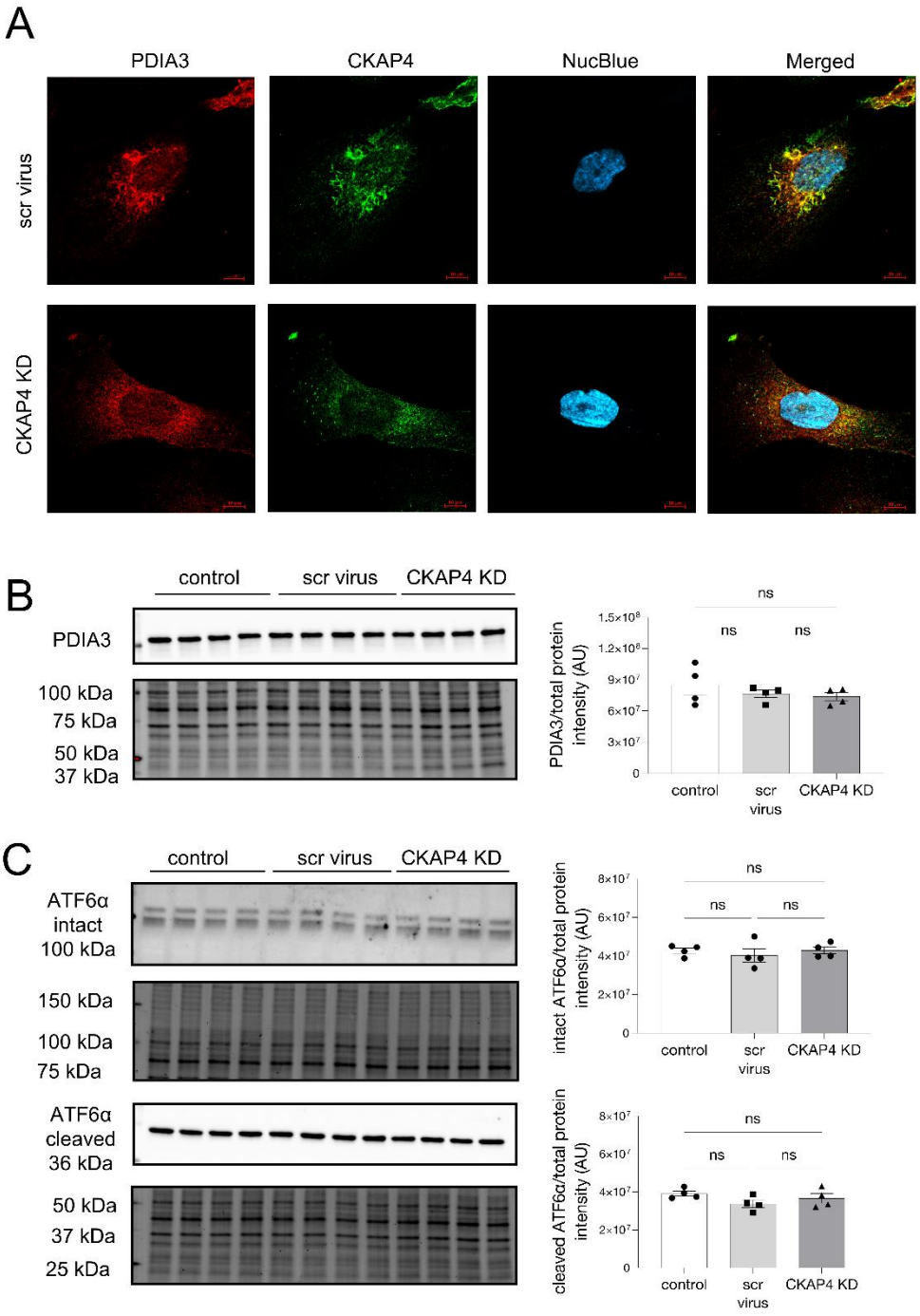
A
PDIA3
CKAP4
NucBlue
Merged
scr virus
CKAP4 KD
B
control
scr virus
CKAP4 KD
PDIA3
100 kDa
75 kDa
50 kDa
37 kDa
PDIA3/total protein intensity (AU)
ns
control
scr virus
CKAP4 KD
C
ATF6α intact 100 kDa
150 kDa
100 kDa
75 kDa
ATF6α cleaved 36 kDa
50 kDa
37 kDa
25 kDa
intact ATF6α/total protein intensity (AU)
cleaved ATF6α/total protein intensity (AU)

Figure 5. CKAP4 knockdown in vitro does not influence the ER in HPODs

Immunofluorescence staining of the ER marker PDIA3 in Scr control and CKAP4 KD HPODs (**A**). Protein expression of PDIA3 was quantified in untreated control, Scr control and CKAP4 KD HPODs using western blot (**B**). Protein expression of ER stress marker intact and cleaved ATF6α in untreated control, Scr control and CKAP4 KD HPODs was quantified by western blot (**C**). The total protein blots used for normalization are shown below each western blot and the quantification graphs are shown on the left side of the panel.

Panel **B**: n=4 per group. Tukey post hoc after one-way ANOVA. ns= non significative. Error bars represent average ± SEM.

AU, arbitrary units; CKAP4, cytoskeleton associated protein 4; PDIA3, protein disulfide-isomerase A3**;** ER, endoplasmic reticulum; KD, knockdown; HPODs, human podocytes.

Figure 6

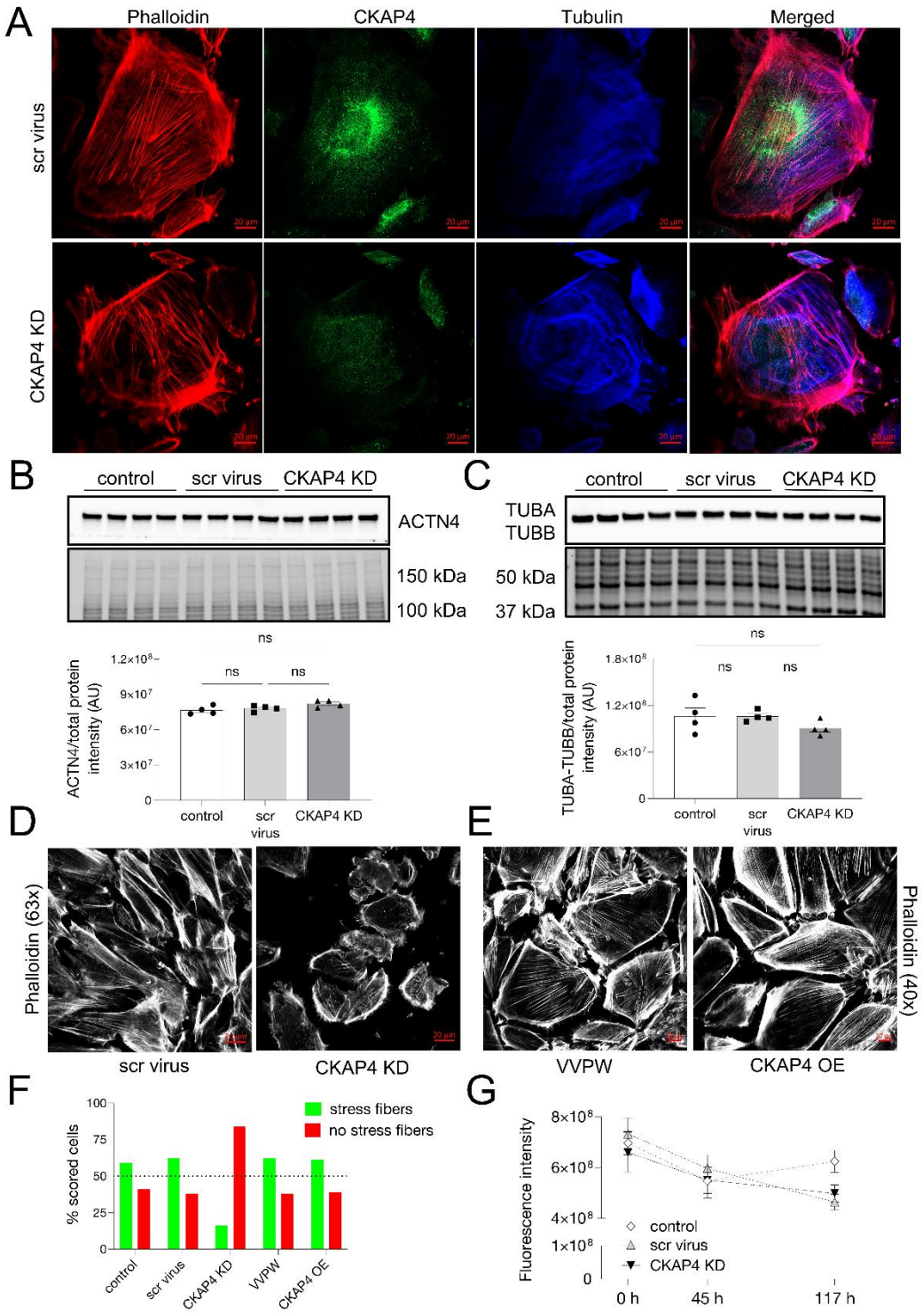
A
Phalloidin
CKAP4
Tubulin
Merged
scr virus
CKAP4 KD
B
control
scr virus
CKAP4 KD
ACTN4
150 kDa
100 kDa
ns
ACTN4/total protein intensity (AU)
control
scr virus
CKAP4 KD
C
control
scr virus
CKAP4 KD
TUBA
TUBB
50 kDa
37 kDa
ns
TUBA-TUBB/total protein intensity (AU)
control
scr virus
CKAP4 KD
D
Phalloidin (63x)
scr virus
CKAP4 KD
E
VVPW
CKAP4 OE
Phalloidin (40x)
F
stress fibers
no stress fibers
% scored cells
control
scr virus
CKAP4 KD
VVPW
CKAP4 OE
G
Fluorescence intensity
control
scr virus
CKAP4 KD
0 h
45 h
117 h

Figure 6. CKAP4 KD in HPODs in vitro alters the cytoskeleton.

Immunofluorescence staining of HPODs with phalloidin (red, actin fibers), tubulin (blue, microtubules) and CKAP4 (green) in scr control and CKAP4 KD. HPODs showed loss of actin stress fibers and rearranged microtubules (**A**). ACTN4 (**B**) TUBA-TUBB (**C**) protein expressions were investigated by western blot. Total protein blots and normalized protein expression graphs are also presented. Representative pictures of phalloidin staining of scr control and CKAP4 KD HPODs (**D**) and VVPW control and CKAP4 OE (**E**). Percentage of cells scored for the presence or absence of stress fibers in both CKAP4 KDs and OE experiments (**F**). HPOD viability in untreated cells, scr control and CKAP4 KD cells from transfection time to 117 h (**G**).

Panel **F**: a minimum of 64 cells per group were scored and percentages are reported in the graph.

Panel **G**: n=8 per time point/group, Friedman test was used, ns.

AU, arbitrary units; CKAP4, cytoskeleton associated protein 4; KD, knockdown; OE, over expression; HPODs, human podocytes; scr, scrambled; ACTN4, alpha-actinin-4**;** TUBA, tubulin alpha**;** TUBB**,** tubulin beta**.**

Figure 7

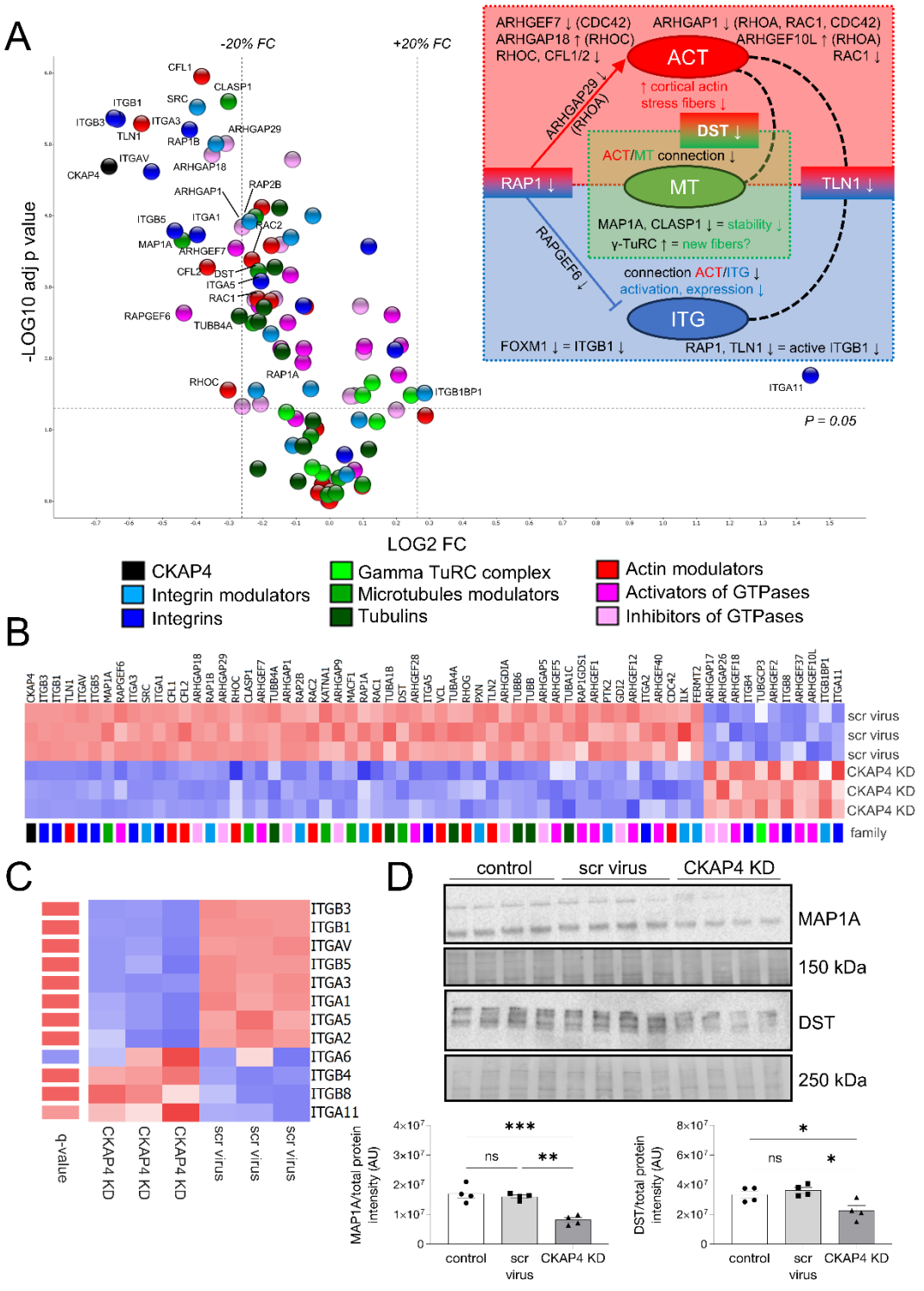
A
-20% FC
+20% FC
-LOG10 adj p value
LOG2 FC
P = 0.05
ARHGEF7 ↓ (CDC42)
ARHGAP18 ↑ (RHOC)
RHOC, CFL1/2 ↓
ARHGAP1 ↓ (RHOA, RAC1, CDC42)
ARHGEF10L ↑ (RHOA)
RAC1 ↓
ACT
↑ cortical actin stress fibers ↓
ARHGAP29 ↓ (RHOA)
DST ↓
ACT/MT connection ↓
RAP1 ↓
MT
TLN1 ↓
MAP1A, CLASP1 ↓ = stability ↓
γ-TuRC ↑ = new fibers?
RAPGEF6 ↓
connection ACT/ITG ↓
activation, expression ↓
ITG
FOXM1 ↓ = ITGB1 ↓
RAP1, TLN1 ↓ = active ITGB1 ↓
CKAP4
Integrin modulators
Integrins
Gamma TuRC complex
Microtubules modulators
Tubulins
Actin modulators
Activators of GTPases
Inhibitors of GTPases
B
scr virus
scr virus
scr virus
CKAP4 KD
CKAP4 KD
CKAP4 KD
family
C
q-value
CKAP4 KD
CKAP4 KD
CKAP4 KD
scr virus
scr virus
scr virus
D
control
scr virus
CKAP4 KD
MAP1A
150 kDa
DST
250 kDa
MAP1A/total protein intensity (AU)
DST/total protein intensity (AU)
control
scr virus
CKAP4 KD

Figure 7. CKAP4 KD influences protein families related to cytoskeleton dynamics.

Volcano plot of selected proteins from the proteomic analysis of CKAP4 KD versus scrambled virus treated HPODs. Dotted lines represent the *P* adjusted threshold of 0.05 (y axis) and fold change thresholds of ± 20% (x axis). Protein variations within these lines were considered not significant and/or not regulated (**A**). The diagram on the upper right side illustrates the dysregulation of ACT (actins), MT (microtubules) and ITG (integrins). Key proteins have modulatory or structural functions in between these groups: RAP1 (ACT and ITG), DST (Distonin, ATC and MT), TLN1 (Talin 1, ITG and ACT).

Heatmap of selected proteins from the proteomics analysis. The color pattern legend identifies protein families in panels A-B. The *p* adjusted filter was set at 0.05 and proteins were sorted by increasing fold change. The color scale ranging from red to blue indicates degrees of upregulation (red) and downregulation (blue), or no regulation (white) (**B**). Heatmap of all the integrins detected in CKAP KD, scrambled virus treated and untreated cells (**C**). Proteins lists are given in Table 3.

Integrins are ranked by increasing fold change (KD vs scrambled). The *q* value scale ranges from blue (ns) to red (<0.05). No *q* value threshold was imposed. Confirmation of the expression of microtubule modulators MAP1A and DST in CKAP4 KD HPODs with western blot (**D**). Total protein blots and normalized protein expression graphs are also presented.

Panel **D**: n=4 per group, Tukey post hoc after one-way ANOVA. * $P<0.05$, ** $P<0.01$, *** $P<0.001$. Error bars represent average ± SEM.

AU, arbitrary units; CKAP4, cytoskeleton associated protein 4; KD, knockdown; scr, scrambled; ITGA6, integrin alpha 6; MAP1A, microtubule associated protein 1A; DST, dystonin.

Figure 8

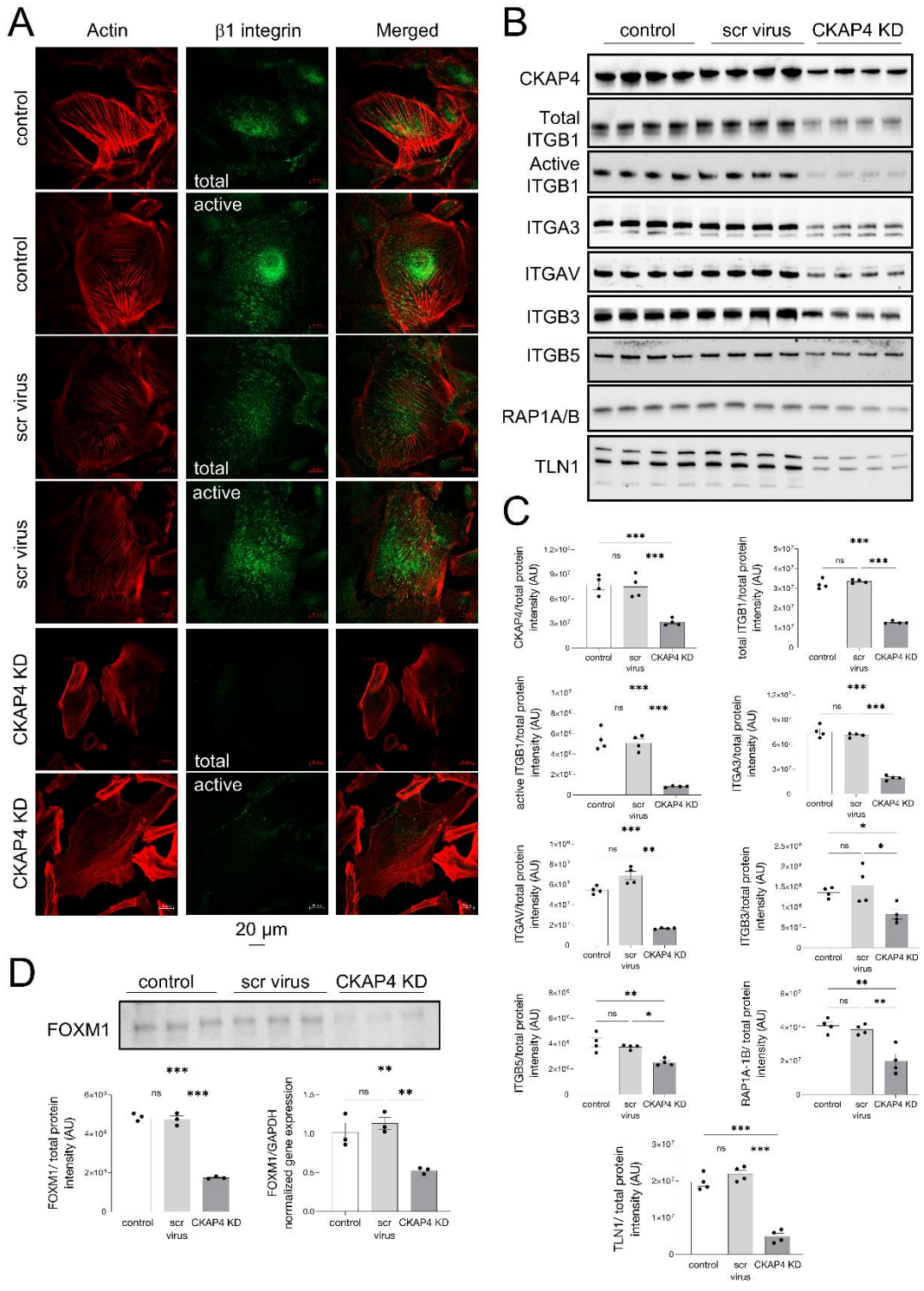
A
Actin
β1 integrin
Merged
control
control
scr virus
scr virus
CKAP4 KD
CKAP4 KD
total
active
total
active
total
active
20 μm
B
control
scr virus
CKAP4 KD
CKAP4
Total ITGB1
Active ITGB1
ITGA3
ITGAV
ITGB3
ITGB5
RAP1A/B
TLN1
C
CKAP4/total protein intensity (AU)
total ITGB1/total protein intensity (AU)
active ITGB1/total protein intensity (AU)
ITGA3/total protein intensity (AU)
ITGAV/total protein intensity (AU)
ITGB3/total protein intensity (AU)
ITGB5/total protein intensity (AU)
RAP1A-1B/ total protein intensity (AU)
TLN1/ total protein intensity (AU)
control
scr virus
CKAP4 KD
ns
***
**
*
D
control
scr virus
CKAP4 KD
FOXM1
FOXM1/ total protein intensity (AU)
FOXM1/GAPDH normalized gene expression

Figure 8. CKAP4 KD causes down regulation of integrins and influences their modulation.

Immunofluorescence images of HPODs (untreated, scrambled virus treated control and CKAP4 KD cells) with phalloidin (actin cytoskeleton, red), total and active β1 integrins (green) (**A**). Western blot of CKAP4, total and active ITGB1, ITGAV, ITGB3, ITGB5, RAP1A/B, and TLN1 are shown (**B**) along with the respective normalized protein expression graphs (**C**). Western blots and relative normalized protein expression graph for FOXM1, together with FOXM1 gene expression (**D**). Unedited/uncropped total protein blots used for normalization calculation are provided as supplementary materials.

Panel **C**: n=4 per group, Tukey post hoc after one-way ANOVA. * $P<0.05$, ** $P<0.01$, *** $P<0.001$. Error bars represent average ± SEM.

Panel **D**: n=3 per group (both gene and protein expression), Tukey post hoc after one-way ANOVA. ** $P<0.01$, *** $P<0.001$. Error bars represent average ± SEM.

AU, arbitrary units; CKAP4, cytoskeleton associated protein 4; FOXM1, forkhead protein M1; KD, knockdown; HPODs, human podocytes; scr, scrambled; ITGB1, integrin beta-1; ITGAV**,** integrin alpha-V; ITGB3**,** integrin beta-3; ITGB5**,** integrin beta-5; RAP1A/B, Ras-related protein Rap-1A/B; TLN1, Talin 1.

Tables

Table 1. CKAP4 expression in glomerular transcriptomic cohorts

Comparison	Fold Change	Q value	Rank
Diabetic Nephropathy vs Healthy Living Donor (24)	0.284	0.0005	***
Diabetic Nephropathy vs Healthy Living Donor (23)	0.713	0.0010	***
IgA Nephropathy vs. Healthy Living Donor (81)	2.082	0.0530	ns
Minimal Change Disease vs Normal Kidney (83)	2.838	0.0750	ns
Vasculitis vs Healthy Living Donor (35)	2.045	0.2730	ns
Lupus Nephritis vs Healthy Living Donor (84)	2.059	0.2780	ns
FSGS[a] vs Normal Kidney (83)	2.121	0.3060	ns
Collapsing FSGS[a] vs Normal Kidney (83)	2.059	0.3770	ns
MN[c] vs Healthy Living Donor (35)	2.022	0.4260	ns
IgA Nephropathy vs Healthy Living Donor (85)	2.013	0.4520	ns
Arterial Hypertension vs Healthy Living Donor (35)	0.498	0.5370	ns
Lupus Nephritis vs Healthy Living Donor (ERBC)	0.475	0.5440	ns
Diabetic Nephropathy vs Healthy Living Donor (35)	0.494	0.5750	ns
Lupus Nephritis vs Healthy Living Donor (35)	0.492	0.6550	ns
IgA Nephropathy vs Healthy Living Donor (35)	0.489	0.7090	ns
FSGS[a] vs Healthy Living Donor (35)	0.486	0.7640	ns
Thin Basement Membrane Disease vs Healthy Living Donor (35)	0.477	0.8070	ns
MCD[b] vs Healthy Living Donor (35)	0.472	0.9250	ns
MCD[b] vs Healthy Living Donor (ERBC)	0.425	0.9500	ns

[a] *FSGS, Focal Segmental Glomerulosclerosis;* [b] *MCD, Minimal change disease;* [c] *MN, Membranous Glomerulonephropathy. The comparisons are ranked by increasing Q values. A Q value <0.05 was considered significant, no fold change threshold was imposed. To our knowledge, ERBC (European Research Biology Center) data are not yet published but can be retrieved at https://www.nephroseq.org/. Q value, false discovery rate adjusted P values, *** Q<0.001. ns, non-significative, p>0.05. IgA, immunoglobulin A.*

Table 2. Ingenuity Pathway analysis of CKAP4 KD vs scrambled virus treated HPODs

Pathway	ratio	P value	z-score
Interleukin-8 Signaling	0.250	5.58E-11	-2.832
Integrin Signaling	0.236	1.24E-10	-3.355
Paxillin Signaling	0.291	1.32E-09	-3.530
Tight Junction Signaling	0.247	1.66E-09	-1.350
Ephrin Receptor Signaling	0.243	1.86E-09	-3.124
Agrin Interactions at Neuromuscular Junction	0.343	8.32E-09	-3.273
Signaling by Rho Family GTPases	0.207	9.12E-09	-2.846
RhoGDI (GDP-dissociation inhibitor) Signaling	0.233	1.05E-08	1.976
Actin Cytoskeleton Signaling	0.208	5.50E-08	-3.280
FAK (focal adhesion kinase) Signaling	0.276	8.71E-08	-3.333
PEDF (pigment epithelium-derived factor) Signaling	0.287	1.07E-07	-1.460
PAK (p21 activating kinase) Signaling	0.270	1.38E-07	-3.000
Relaxin Signaling	0.226	2.75E-07	-1.279
Acute Phase Response Signaling	0.219	2.88E-07	0.962
Interleukin-1 Signaling	0.272	3.47E-07	-2.400
Tec Kinase Signaling	0.214	7.24E-07	-2.200
Rac Signaling	0.241	1.00E-06	-3.024
Ephrin B Signaling	0.288	1.07E-06	-1.807
Death Receptor Signaling	0.261	1.35E-06	0.209
Inhibition of Angiogenesis by TSP1 (Thrombospondin 1)	0.406	1.66E-06	1.414

Pathways are ranked by increasing P value. P<0.05 is considered significant. The column ratio identifies the pathway coverage (found/total). Z-score identifies directionality and extent of the regulation.

Table 3. List of proteins for proteomics analysis

Protein family	Proteins
Actin modulators	CFL1, CFL2, PFN1, PFN2, PLEC, CDC42, RAC1, RAC2, RAC3, RHOA, RHOB, RHOBTB1, RHOBTB2, RHOC, RHOD, RHOG, RHOH, RHOJ (TCL), RHOQ (TC10), RHOU (WRCH), RHOV (WRCH2), RIF (RHOF), RND1 (RHO6), RND2 (RHON), RND3 (RHOE), TLN1, TLN2, VCL
Gamma TuRC complex [a]	TUBG1, TUBG2, TUBGCP2, TUBGCP3, TUBGCP4, TUBGCP5, TUBGCP6
GTPases activation	ARHGEF1, ARHGEF2, ARHGEF5, ARHGEF6, ARHGEF7, ARHGEF10, ARHGEF10L, ARHGEF11, ARHGEF12, ARHGEF17, ARHGEF18, ARHGEF26, ARHGEF28, ARHGEF37, ARHGEF40, RAP1GDS1, RAPGEF2, RAPGEF3, RAPGEF6
GTPases deactivation	ARHGAP1, ARHGAP5, ARHGAP6, ARHGAP9, ARHGAP10, ARHGAP15, ARHGAP17, ARHGAP18, ARHGAP19, ARHGAP21, ARHGAP22, ARHGAP23, ARHGAP24, ARHGAP26, ARHGAP27, ARHGAP28, ARHGAP29, ARHGAP30, ARHGAP32, ARHGAP33, ARHGAP35, ARHGAP42, RACGAP1, ARHGDIA, ARHGDIB, GDI2
Integrins	ITGA1, ITGA2, ITGA3, ITGA4, ITGA5, ITGA6, ITGA8, ITGA11, ITGAL, ITGAV, ITGB1, ITGB2, ITGB3, ITGB4, ITGB5, ITGB6, ITGB8
Integrins modulators	FERMT2, FERMT3, ILK, ILKAP, ITGB1BP1, PTK2, PXN, RAP1A, RAP1B, RAP2A, RAP2B, SRC
Microtubules modulators	APC, CLASP1, CLASP2, CRMP2 (DPYSL2), DNAH17, DNAH9, DST, DYNC1H1, DYNC2H1, KATNA1, KIN13A/B, MACF1, MAP1A, MAP1B, MAP2, MAP6, MAPT, MARK4, MCAK (KIF2C)
Tubulins	TUBA1A, TUBA1B, TUBA1C, TUBA3C, TUBA3D, TUBA3E, TUBA4A, TUBA8, TUBAL3, TUBB, TUBB2A, TUBB2B, TUBB2C, TUBB3, TUBB4A, TUBB4B, TUBB6, TUBD1, TUBE1

[a] *TuRC, gamma-tubulin ring complex.*